

5-1-2015

Laser induced breakdown spectroscopy of martian breccia Northwest Africa 7034: comparison with Mars Science Laboratory results

Suzanne Gordon

Follow this and additional works at: https://digitalrepository.unm.edu/eps_etds

Recommended Citation

Gordon, Suzanne. "Laser induced breakdown spectroscopy of martian breccia Northwest Africa 7034: comparison with Mars Science Laboratory results." (2015). https://digitalrepository.unm.edu/eps_etds/31

This Thesis is brought to you for free and open access by the Electronic Theses and Dissertations at UNM Digital Repository. It has been accepted for inclusion in Earth and Planetary Sciences ETDs by an authorized administrator of UNM Digital Repository. For more information, please contact disc@unm.edu.

Suzanne Gordon

Candidate

Earth and Planetary Science

Department

This thesis is approved, and it is acceptable in quality and form for publication:

Approved by the Thesis Committee:

Dr. Horton Newsom, Chairperson

Dr. Carl Agee

Dr. Francis McCubbin

Dr. Louis Scuderi

**LASER INDUCED BREAKDOWN SPECTROSCOPY OF
MARTIAN BRECCIA NORTHWEST AFRICA 7034:
COMPARISON WITH MARS SCIENCE LABORATORY
RESULTS**

by

SUZANNE GORDON

**B. S., SPACE SCIENCES, FLORIDA INSTITUTE OF
TECHNOLOGY
DECEMBER 2011**

THESIS

Submitted in Partial Fulfillment of the
Requirements for the Degree of

**Master of Science
Earth and Planetary Science**

The University of New Mexico
Albuquerque, New Mexico

May, 2015

ACKNOWLEDGEMENTS

I would like to acknowledge my advisor, Horton Newsom, for his guidance throughout my degree program and Nina Lanza, who helped refine this thesis. I would also like to recognize Alison Santos, Carl Agee, and Francis McCubbin for their insight in giving direction to this project. Many thanks to Lou Scuderi, Sam Clegg, Roger Wiens, Mike Spilde, Rhonda McIlroy, Elena Dobrica, and Kathleen Vander Kaaden for their advice and assistance with instrumentation, data analysis, and interpretation. Special thanks for the invaluable support from my fiancé, RJ Montaña, and my parents, Tim and Marilu Gordon.

**LASER INDUCED BREAKDOWN SPECTROSCOPY OF MARTIAN BRECCIA
NORTHWEST AFRICA 7034: COMPARISON WITH MARS SCIENCE
LABORATORY RESULTS**

by

Suzanne Gordon

B.S., Space Sciences, Florida Institute of Technology, 2011
M.S., Earth and Planetary Science, University of New Mexico, 2015

ABSTRACT

The Mars Science Laboratory (MSL) rover is utilizing laser-induced breakdown spectroscopy (LIBS) instrumentation to determine compositions of rocks shot in Gale crater, Mars, from a distance of 1.56-7 meters. At the same time, martian breccia meteorite Northwest Africa (NWA) 7034 was analyzed with the ChemCam engineering model laboratory LIBS instrument at Los Alamos National Laboratory (LANL) at a 1.6 m standoff distance under 7 Torr CO₂. Each LIBS location was pulsed with 150 shots at 3 Hz and 13.5 mJ/pulse. Comparison of NWA 7034 LIBS results with the bulk composition acquired with electron probe microanalysis (EPMA) show agreement within LIBS instrument error. Comparison of NWA 7034 data with targets from Gale show chemical and textural similarities. This study helps bridge the gap between Mars *in situ* and martian meteorite data by using LIBS data to determine compositions of heterogeneous rock samples outside the compositional range previously observed on Mars.

TABLE OF CONTENTS

LIST OF FIGURES.....	vii
LIST OF TABLES.....	ix
1. INTRODUCTION	1
1.1 Martian meteorites and NWA 7034	1
1.2 LIBS technique and previous studies	4
1.3 Purpose of this study	7
2. METHODS.....	8
2.1 LIBS experimental setup	8
2.2 LIBS analytical methods	11
2.3 ChemCam observations.....	15
3. RESULTS.....	22
3.1 Summary.....	22
3.2 LIBS and EPMA table summaries	22
4. DISCUSSION.....	28
4.1 NWA 7034 LIBS results interpretation	28
4.2 Comparison of NWA 7034 LIBS and EPMA results.....	38
4.3 LIBS sampling study	40
4.4 Comparison of NWA 7034 and ChemCam targets	54
5. CONCLUSION	58

6. REFERENCES59

LIST OF FIGURES

Figure 2.1 NWA 7034 First Round LIBS Locations	10
Figure 2.2 NWA 7034 Second Round LIBS Locations	10
Figure 2.3 NWA 7034 EPMA Locations.....	16
Figure 2.4 Gale Crater Context Map.....	17
Figure 2.5 MSL Traverse Map.....	19
Figure 2.6 Jake M Images.....	19
Figure 2.7 Ashuanipi Images	20
Figure 2.8 La Reine Images	20
Figure 2.9 Harrison Images	21
Figure 4.1 Total Alkali vs. Silica diagram comparing Mars data.....	30
Figure 4.2 NWA 7034 Clasts 9 and 10 BSE Images	32
Figure 4.3 Round 1 LIBS Locations 9 and 10 Comparison	33
Figure 4.4 Round 1 LIBS Locations 9 and 10 Shot-to-Shot Distribution.....	34
Figure 4.5 Normal Probability Plots for LIBS Location 9 and 10 Data	35
Figure 4.6 Z-score Difference Spectrum of LIBS Round 1, Location 10	38
Figure 4.7 Al/Si vs. (Fe+Mg)/Si of NWA 7034 Data from Multiple Sources.....	40
Figure 4.8 BSE Image of Matrix Surrounding LIBS Round 1, Location 2	43
Figure 4.9 Si, Mg, and Na Maps of LIBS Round 1, Location 2 Matrix.....	45

Figure 4.10 BSE Image of LIBS Round 1, Location 10 Clast.....	48
Figure 4.11 Si, Mg, and Na Maps of LIBS Round 1, Location 10 Clast.....	48
Figure 4.12 BSE Image of Matrix and Clast Area	50
Figure 4.13 Si, Mg, and Na Maps of Matrix and Clast Area.....	51
Figure 4.14 Sammon's Map of NWA 7034 and Select ChemCam Targets.....	55

LIST OF TABLES

Table 3.1 LIBS Results	22
Table 3.2 EPMA Results	23
Table 3.3 Jake M LIBS Results	23
Table 3.4 Ashuanipi LIBS Results	24
Table 3.5 La Reine LIBS Results	24
Table 3.6 Harrison LIBS Results	25
Table 4.1 Si, Mg, Na, Al, and Ca Pixel Intensities for EDS Images	49
Table 4.2 Si, Mg, Na, Al, and Ca LIBS Spectral Peak Areas	51
Table 4.3 Color-coded Jake M Round 1 LIBS Results	53
Table 4.4 Color-coded Jake M Round 2 LIBS Results	54

1. INTRODUCTION

1.1 *Martian meteorites and NWA 7034* The first meteorites discovered to be from Mars were classified as SNCs (Shergottite-Nakhlite-Chassignite, after three meteorites with related compositions) and were thought to represent the average basaltic composition of the surface of Mars (McSween, 1985). The SNC meteorites have been divided into three groups: basaltic, pyroxene and plagioclase cumulate Shergottites; clinopyroxene cumulate Nakhlites; and dunite Chassignites (Papike et al., 2009). Observations of Mars from orbiter and lander missions have shown, however, that the martian crust is more alkali-rich than the SNC meteorites suggest (e.g., Gellert et al., 2006; Boynton et al., 2007). The discovery of a small number of non-SNC martian meteorites shows evidence of the diversity of martian materials.

The martian meteorite examined in this study, NWA (Northwest Africa) 7034, is a non-SNC meteorite that in bulk closely matches the composition of the martian surface seen by the MER (Mars Exploration Rover) *Spirit* at Gusev crater, Mars, and its small-scale variation of felsic and mafic materials mirrors the range of compositions seen by MSL in Gale crater. NWA 7034 is also a unique martian meteorite in that it is a water-rich basaltic breccia (~6000 ppm as compared to the average of ~600 ppm for SNCs) (Agee et al., 2013) with a composition and texture that has not been seen in any other martian meteorites discovered to date. The first piece of NWA 7034 was found in Morocco and purchased from Aziz Habibi, a meteorite dealer, by Jay Piatek. Paired meteorites include NWA 7533 and NWA 7475 (Humayun et al., 2013 and Korotev et al., 2013). The interior of the meteorite is dark in color, with clast lithologies ranging from

light toned to dark toned and compositions from alkali-rich basalt to trachyandesite. This brecciated sample consists of multiple clasts of different igneous rock types that were aggregated in either a sedimentary lithification or volcanic event. This is the first martian sample that is not a primary igneous material to be studied on Earth. The Rb-Sr and Sm-Nd dating reported by Agee et al. (2013) gave an age of 2.089 ± 0.081 Ga for the whole rock, placing its formation in the early Amazonian (3.0 Ga to present) epoch. However, Humayun et al. (2013) studied U-Pb dating in zircons in the meteorite and measured a formation age of 4.428 ± 0.025 Ga (in the Pre-Noachian time period before 4.1 Ga), confirming the polymict nature of the breccia. Cartwright et al. (2014) studied the atmospheric signatures of NWA 7034 and determined that excess ^{136}Xe produced from fission tracked a ^{238}U age similar to the zircon age from Humayun et al. (2013) at 4.15 ± 0.035 Ga. Gas retention ages for the K-Ar dating systems reported in Cartwright et al. (2014) have an upper limit of 1.56 Ga, consistent with the disturbance at 1.721 ± 0.085 Ga seen in the zircons. The U-Th/He retention age in Cartwright et al. (2014) is ~ 170 Ma and indicates severe radiogenic ^4He loss at that time. This time stamp is similar to the formation age for most of the Shergottites, which the authors suggest is an indication that a single event was responsible for both the crystallization of the Shergottite meteorites and the radiogenic ^4He loss of NWA 7034. Cartwright et al. also note a trapped gas component in NWA 7034 that is similar to the modern martian atmosphere, suggesting that the origin of the meteorite is either from a large meteoroid with an atmosphere and/or from the martian surface. The isotope data are consistent with a breccia or sediment containing early crustal components that have been partially modified by later processes.

NWA 7034 was first reported to be a monomict breccia with a range of feldspar and pyroxene compositions indicating a common petrologic origin during a single volcanic event. However, further study of the clasts in the meteorite show a polymict signature with up to six lithologies. Humayun et al. (2013) suggested that exsolution in pyroxenes and alkali feldspars indicated a plutonic origin for those clasts, while the other clasts formed by fractional crystallization. Santos et al. (2015) classified four igneous lithologies in the meteorite: basalt, basaltic andesite, trachyandesite, and a lithology consisting of high Fe, Ti, and P (FTP). The basaltic category includes the three subcategories: high and low calcium pyroxene, low calcium pyroxene, and low calcium pyroxene and pigeonite groups. Electron microprobe analysis (EPMA) studies of the lithologies have revealed different cooling rates, igneous textures, and trace element abundances (Santos et al. 2015). Recently, work by McCubbin et al. (2014) examined the alteration of the sedimentary clasts in the meteorite for morphological evidence of the clasts' histories. They found evidence of transport through an analysis of brecciated lithic clast shapes, as well as evidence of alteration by martian crustal fluids, which may indicate fluvial transport of these non-igneous clasts, which consist of fine grained matrix surrounding larger mineral fragments, prior to their inclusion in the meteorite material. Because this meteorite matches more closely the average surface composition of Mars than any other martian meteorite and possibly contains evidence of interaction with the martian surface environment (e.g., atmosphere and groundwaters), it provides an excellent test case to better understand in situ measurement of new types of martian materials by the ChemCam (Chemistry and Camera) LIBS instrument on board MSL.

1.2 LIBS technique and previous studies Laser induced breakdown spectroscopy (LIBS) has been used for spectrochemistry since the mid-1900s, and it is currently being used for geological applications on the Mars Science Laboratory (MSL) *Curiosity* rover. The LIBS technique can provide quantitative elemental compositions of major and trace elements (Clegg et al., 2009; Wiens et al., 2012). ChemCam LIBS observations are normally acquired as a two-dimensional grid, called a raster, of locations with 30 to 50 nanoseconds-long laser pulses per location; however, the 1067 nm Nd:KGW laser can acquire up to 1000 shots at one location and profile up to 1 mm of depth into a rock, with multiple ChemCam targets observed on a single sol, or martian day. Each laser pulse ablates a small volume of material and excites the atoms of the target to higher electronic states. When these atoms return to their resting state they release photons at characteristic wavelengths, creating bright plasma. Some of the light from the plasma is collected by a telescope and directed to a demultiplexer connected to three spectrometers inside the body of the rover collecting light at wavelengths ranging from ~240 to 900 nm. The raw spectra are pre-processed to remove noise and the electron continuum, and then they are corrected for distance and instrument response (Wiens et al., 2013). Elemental abundance is quantified using both univariate and multivariate analysis techniques such as peak fitting and partial least squares (PLS) (e.g., Clegg et al., 2009; Wiens et al., 2013). Both of these techniques are discussed in Section 2.

Multiple laboratory tests have been conducted to verify the ability of LIBS to characterize terrestrial rocks (e.g., Clegg et al., 2009; Tucker et al., 2010; Lanza et al., 2012). LIBS spectra are affected by numerous environmental conditions, leading to differences in data obtained on Earth and Mars. Atmospheric effects influence LIBS

plasma intensity through interactions between the breakdown products of the atmosphere and the ablated surface material in the plasma. Atmospheric pressure affects the size of the plasma created after each LIBS pulse, with martian atmosphere having close to the ideal pressure wherein the plasma is large enough that it can be effectively analyzed from a distance but not so large that it diffuses before it is analyzed. The standoff distance also affects the emission intensity of the plasma. ChemCam (Chemistry and Camera), the LIBS instrument on board MSL, targets rocks and soils from 1.56 to 7 meters away; past 7 meters the signal-to-noise ratio becomes too low to obtain useful data. LIBS is well suited to field geology settings due to its ability to quickly and effectively sample targets at a distance. The LIBS sample size (350-500 microns, depending on standoff distance) allows for bulk chemical analysis on fine-grained targets and mineral identification of large grains in coarse rock targets (Wiens and Maurice, 2015). Repeated laser pulses at the same analysis location also allow for depth profiling of rock targets with coatings. In addition to the LIBS, ChemCam also has a Remote Micro-Imager (RMI) that is capable of taking sub-millimeter resolution images of its targets before and after LIBS analysis to provide a visual context for the compositional data. These advantages led to the selection of the ChemCam instrument on board the MSL *Curiosity* rover (Wiens et al., 2012 and Maurice et al., 2012).

Because LIBS is a relatively new method of studying geological materials, studies were completed prior to the launch of MSL testing the ability of LIBS study whole rock samples and extraterrestrial materials. Thompson et al. (2006) used LIBS to analyze the martian Shergottite meteorites Dar al Gani 476 and Zagami as analogs of materials that might be encountered by a rover on Mars. With these data they were able to predict the

compositions of these meteorites as reported in the literature within 12 oxide weight percent error. The authors also tested whether LIBS could distinguish between andesitic and basaltic compositions by analyzing an andesite standard and comparing the resulting spectra with those of the basaltic martian Shergottites and were able to predict the andesite composition within 9 oxide weight percent error. These results show that while there are larger uncertainties associated with LIBS than with traditional analysis methods such as electron probe microanalysis (EPMA), the technique can still be used to produce reliable chemical compositions. LIBS can be used to study a variety of geological materials such as rock varnish and weathering rinds (Lanza et al., 2012), sulfate minerals (Sobron et al., 2012), and ferric salts in frozen solutions (Schröder et al., 2012). Effective analysis of these materials on Mars would show evidence of long-standing water and potentially habitable environments, which aligns with the mission goals of MSL. Most recently, Dell'Aglio et al. (2014) applied a calibration-free LIBS technique to analyze a chondrule inside a chondritic meteorite and kamacite and taenite crystals within a Widmanstätten pattern in an octahedrite iron meteorite. The authors compared LIBS and electron microprobe data of one sample of each meteorite type, as well as predicted the composition of each LIBS target using a calibration-free method, to demonstrate that LIBS is a mature enough analysis technique to effectively analyze astromaterials. Along with laboratory and field studies using LIBS instrumentation, McCanta et al. (2013) investigated the requirements for obtaining reasonable bulk chemical compositions of mineral assemblages with the ChemCam LIBS technique using a strictly theoretical approach. They concluded that when grain size is smaller than LIBS beam size, only ten analyses are needed in a two-dimensional theoretical sample to deliver a precise and

accurate bulk composition. They also noted that in cases where beam size is similar to or smaller than grain size, an accurate analysis of heterogeneous materials is possible. In this study we extend and test that approach using data for an actual martian sample with sedimentary affinity.

1.3 Purpose of this study The purpose of this study is to determine the capability of LIBS to observe chemical differences in samples like NWA 7034 that the rover may analyze in Gale crater. Analysis of NWA 7034 with the ChemCam engineering model as well as with more widely used terrestrial laboratory methods can clarify results from ChemCam on martian targets that are texturally and/or chemically similar to NWA 7034. Understanding the variation in LIBS data obtained on heterogeneous geological targets provides an important measure of how sampling location and frequency will affect results obtained from ChemCam analyses on Mars, leading to a more accurate understanding of the rock and soil formation history of Gale crater in particular and Mars overall.

2. METHODS

2.1 LIBS experimental setup As a test of the LIBS technique in characterizing a heterogeneous martian sample in a terrestrial lab, the LIBS instrument at Los Alamos National Laboratory (LANL) was used to conduct observations on a martian meteorite, basaltic breccia Northwest Africa (NWA) 7034. While effort was taken to ensure the LIBS instrumentation on MSL exactly matches that at Los Alamos, some inherent differences evolve from comparing the two techniques. First, the chamber at Los Alamos is filled with pure CO₂ and kept at constant temperature and humidity, whereas the atmosphere during ChemCam observations has differing temperature and humidity depending on the time of observation. The sample is also prepared differently at Los Alamos in comparison to the field targets at Gale crater. Targets on Mars also have uneven surfaces and may be covered in dust, however the application of up to five LIBS shots in the same location is used to remove dust on the target. The sample of NWA 7034 used in this study was saw-cut before the first round of LIBS and polished and a carbon coated in the second round of LIBS, thus showing a relatively flat face of the interior of the meteorite. Distance to target is another difference between Los Alamos and Gale crater LIBS observations, with MSL targets shot at a range of distances up to 7 meters while NWA 7034 was shot at a set distance of 1.6 meters. The final difference between MSL and LANL LIBS is the angle at which targets are shot. The ChemCam laser on MSL is located about 2 meters off the ground, thus creating a shooting angle between 16° and 52° depending on the distance to the target, while the LANL laser is located on the same plane as the sample and therefore shoots the sample head-on. ChemCam LIBS data

are pre-processed with a solid angle correction, though (Wiens et al., 2013), so this difference should not affect the results of this study.

The sample of NWA 7034 (Figure 2.1) used in this study is a slab about 12 mm wide that was cut from the ~320 g whole rock, which is on deposit at the University of New Mexico Institute of Meteoritics. The sample was placed in the chamber 1.6 m from the laser and rotated by hand to target ten different locations. The first location was a test of the visibility of the laser pit on the sample; 50 shots were fired at 12 mJ per pulse at a repetition rate of 3 Hz to test visibility of the LIBS spot for confirmation of what section of the sample was hit. The other nine locations were pulsed with 150 laser shots each to ensure the locations could be seen with the naked eye. The 1400 LIBS spectra (50 for one location, 150 each for the remaining nine locations) were collected in the same way as ChemCam LIBS spectra (described above and by Maurice et al., 2012). After the first round of LIBS, the sample was polished and carbon-coated, and electron microprobe analysis (EPMA) and energy dispersive spectroscopy (EDS) mapping were performed on the sample. EPMA and EDS techniques will be discussed in the next section. After EPMA and mapping, the carbon coated sample was analyzed with another round of LIBS at the same conditions as the first round; however, due to instrument limitations, instead of analyzing each laser location for one set of 150 pulses, each location was analyzed with three sets of 50 pulses. The only difference between one set of 150 shots and three sets of 50 shots in a single location is lag time, and this time difference should not have affected the LIBS results because analysis of a sample in a vacuum-pumped chamber is not time-sensitive. A total of eight locations were analyzed in the second round of LIBS (Figure 2.2), for a grand total of 18 LIBS locations on the face of the sample.

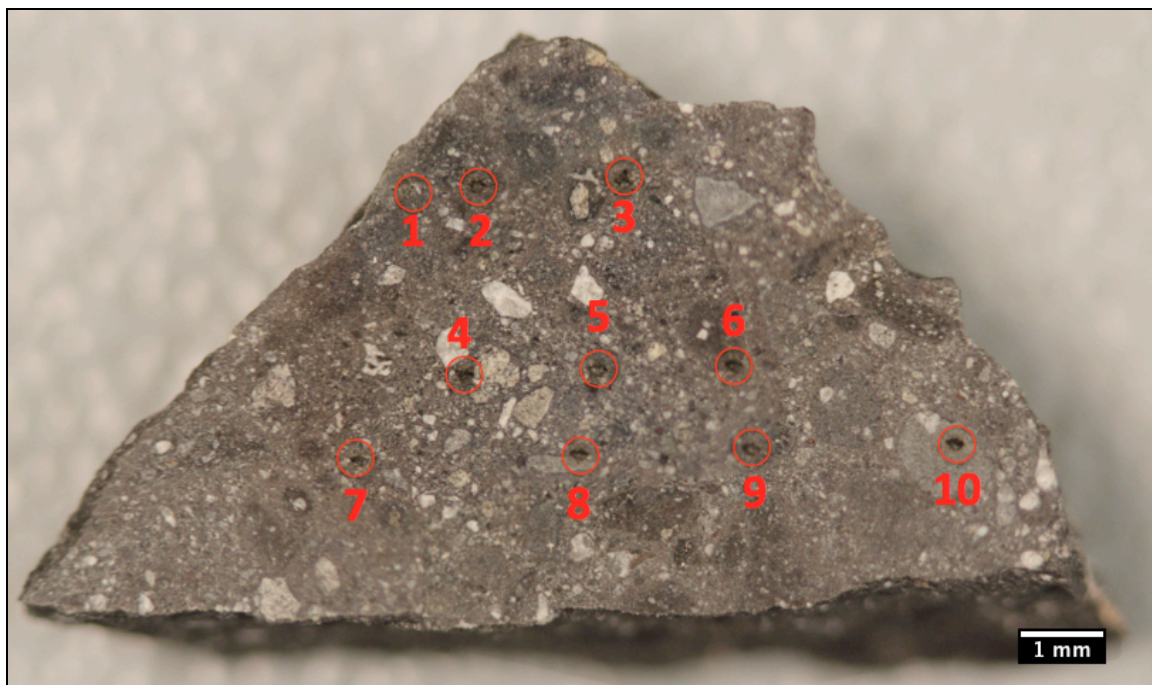


Figure 2.1 First round of LIBS locations for the NWA 7034 sample. Location 1 was pulsed with 50 shots, and all other locations were pulsed with 150 shots to make the LIBS hole more visible.

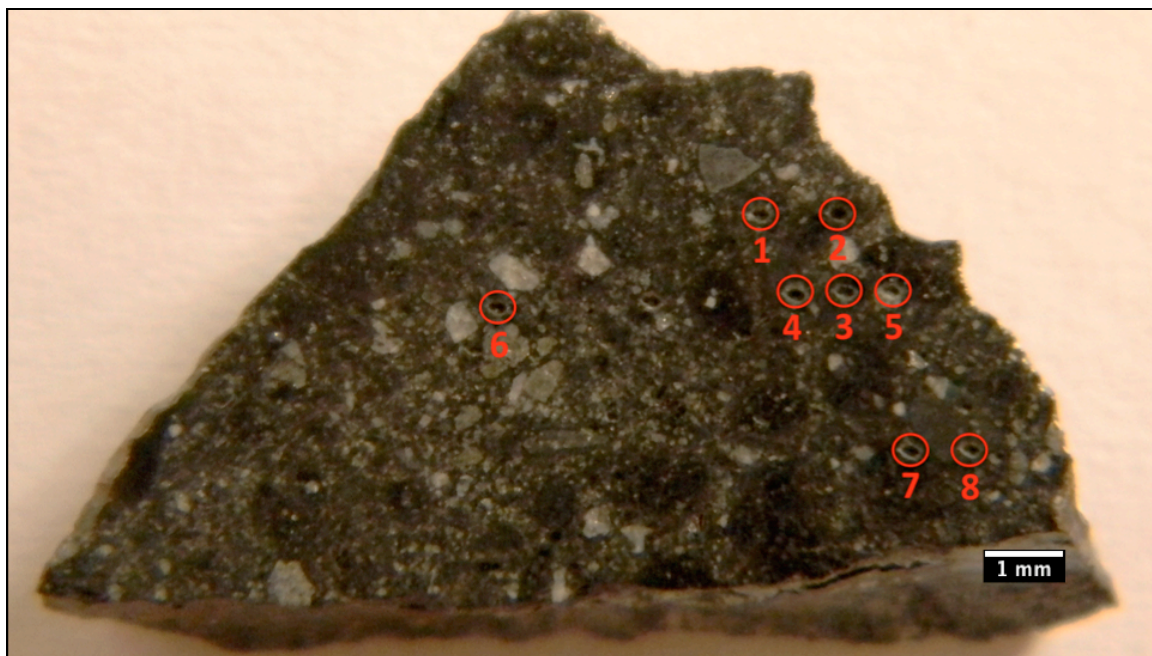


Figure 2.2 Second round of LIBS locations for the NWA 7034 sample. Each location was pulsed with three sets of 50 laser shots.

2.2 LIBS analytical methods The resulting emission spectra for SiO₂, TiO₂, FeO, and Na₂O were analyzed using an updated version of the MSL prime mission Partial Least Squares (PLS)-1 training set created for the ChemCam instrument, which includes 482 test samples of varying petrologic types (Clegg et al., 2014). PLS is a type of multivariate analysis commonly used to analyze complex systems. This method requires *a priori* knowledge of the possible range of compositions of the unknown sample being analyzed, so that a calibration set encompassing the appropriate range can be used to accurately quantify the major element concentrations of the unknown sample. Multivariate analysis differs from univariate analysis methods such as peak fitting because PLS uses the entire LIBS spectra to determine the composition of each element, which takes into account matrix effects that are ignored by univariate analysis. The new calibration set is comprised of igneous rocks ranging in TAS (total alkali versus silica) compositions spanning all classifications as well as metamorphic and sedimentary compositions including clays, metasediments, and clastic sediments. The new range of rock types has improved the overall coverage of SiO₂ compositions by 30%, FeO compositions by 84%, and Na₂O compositions by almost 700% over analyses using the original calibration set. There was little to no improvement of coverage for Ti (18%); however, the major discrepancies in PLS results usually stem from questionable Si, Fe, and Na calculations, so overall this new calibration set shows a vast improvement on predicted values. To prepare the spectra for PLS, each spectral channel (UV, VIS, VNIR) was normalized by dividing each pixel's intensity by the total integrated intensity for that spectral channel. As explained by Clegg et al. (2009), PLS assigns the spectra as

independent X variables and elemental compositions as dependent Y variables, and then correlates the two using Equation (2.1):

$$Y = XB \quad (2.1)$$

where B is a matrix that describes the relationship between pixel intensities and elemental response. By definition, PLS-1 uses only one Y variable is used in the analysis, whereas PLS-2 uses two variables. Tucker et al. (2010) determined PLS-1 to be comparable to PLS-2 in giving accurate predictions, and PLS-1 is advantageous with shorter calculation times. PLS-1 on this sample of NWA 7034 was performed using ChemCam software available only to team members; however, there are many free programs that perform PLS as well. While the LIBS instrument records atomic fractions of elements in each plasma observation, data are reported as oxides as is customary in the reporting of geochemical data. It is important to note that atomic fractions and oxide weight percentages of elements are not the same due to stoichiometry, so conversion factors are used to change data to atomic fractions before fitting calibration curves. Calibration curves are created as regression plots showing the statistical correlation between elemental variations and observed variations in each pixel of the spectrum. From these calibration curves, PLS analysis correlates spectral changes with elemental compositions according to Equation (2.2):

$$Y = b_0 + b_1X_1 + \dots + b_kX_k + e \quad (2.2)$$

where Y is the elemental composition, X_n is the spectral channel, b_n is the regression coefficient, and e is the error matrix. After PLS analysis for the unknown is completed, cross-validation is performed using a leave-one-out method of treating one of the

standards as an unknown and using the PLS model to confirm the composition of the “unknown known” to make the PLS calculation more robust. Because the new calibration set for ChemCam PLS has over 450 standards, this process takes much longer than when using the old calibration set, but it yields much more accurate results. PLS results for NWA 7034 and the ChemCam targets used in this study are listed in Section 3. Clegg et al. (2009) have shown that PLS is effective at compensating for chemical matrix effects, and the authors speculate the reason is because PLS uses statistics to identify changes observed in the plasma as a result of variations in the matrix, thus allowing removal of chemical matrix effects on a location-to-location basis. The error accompanying any PLS analysis is called the Root Mean Square Error of Prediction, or RMSEP:

$$RMSEP = \sqrt{\frac{\sum_{i=1}^n d_i^2}{n}} \quad (2.3)$$

where n is the number of standards, i is the estimated value, and d is the difference between the predicted and estimated values (Fabre et al., 2014). This error is the standard deviation of the LIBS predictions to the known compositions (Tucker et al., 2010), and its value varies depending on which element is being predicted. All RMSEP errors are reported along with the LIBS data in the results tables in Section 3.

LIBS results for Al_2O_3 , MgO , MnO , and K_2O were obtained using univariate analysis, which was chosen over PLS for these oxides because it gave the closest values to the EPMA values reported by Agee et al. (2013). Assuming a linear relationship between the intensity of stable emission lines for a given element and that element's abundance at the sampling location, a univariate calibration can be made using a smaller

amount of known samples than needed for PLS analysis. However, because analysis is only performed on specific emission peaks, the univariate method does not take matrix effects into account. The calibration targets used in this univariate analysis are the ChemCam calibration targets (CCCTs) onboard the *Curiosity* rover (Fabre et al., 2011). In univariate analysis, the most stable emission peaks for each element are used to calculate a total peak area for the element, which is then translated to a predicted composition as calibrated by the CCCTs. Because the LIBS data on NWA 7034 were taken in a laboratory environment at LANL and the CCCT LIBS data were taken *in situ* on Mars, there is a discrepancy between the two data sets for some elements. However, Al, Mg, Mn, and K show results in agreement with EPMA compositions of NWA 7034 and thus will be used in this study. Work is ongoing within the ChemCam team to determine the best analysis method for ChemCam LIBS results; however, this discussion lies outside the scope of this project.

Following the first round of LIBS observations on NWA 7034, the sample was polished and carbon coated, and electron probe microanalysis (EPMA) using the JEOL JXA 8200 electron microprobe at UNM was completed on the two clasts shot by LIBS (labeled 9 and 10 in Figure 2.1) to compare the two data analysis methods. EPMA uses wavelength-dispersive spectroscopy (WDS) to acquire quantitative chemical abundances on a scale of tens of microns. For this study, EPMA was used in grids of 4x4 points to cover roughly the same scale as a LIBS spot. Analysis was also done on three light-colored clasts in the meteorite (Figure 2.3). Following the EPMA observation, an element map of the whole sample was made using electron dispersive spectroscopy (EDS) on the JEOL JSM 5800LV scanning electron microscope (SEM) at UNM at 30 kV and 32nA.

The SEM uses an electron beam to create backscatter electron intensities corresponding to elemental concentrations across the surface of a sample, creating a full image of the sample. Brighter colors in each element map indicate a higher abundance of that element, and darker colors indicate lower abundances. The EDS images are discussed in-depth in Section 4. A second round of LIBS shots were then taken on the carbon-coated NWA 7034 sample, and their compositions were determined with the same data analysis techniques used on the first round of LIBS. The results are presented in the following section and discussed in the Section 4.

Energy dispersive spectroscopy (EDS) element maps were created after LIBS and EPMA analyses. EDS maps show relative x-ray intensities of selected elements over the area of the sample. EDS data were obtained with the JEOL JSM 5800LV scanning electron microscope (SEM) at the University of New Mexico using a 30 kV accelerating voltage, 32 nA beam current, and 150x magnification. The resulting images are created with approximately 12.5 microns per pixel, with pixel intensities directly correlating to the element's abundance in the image. The images are discussed in Section 4.3.

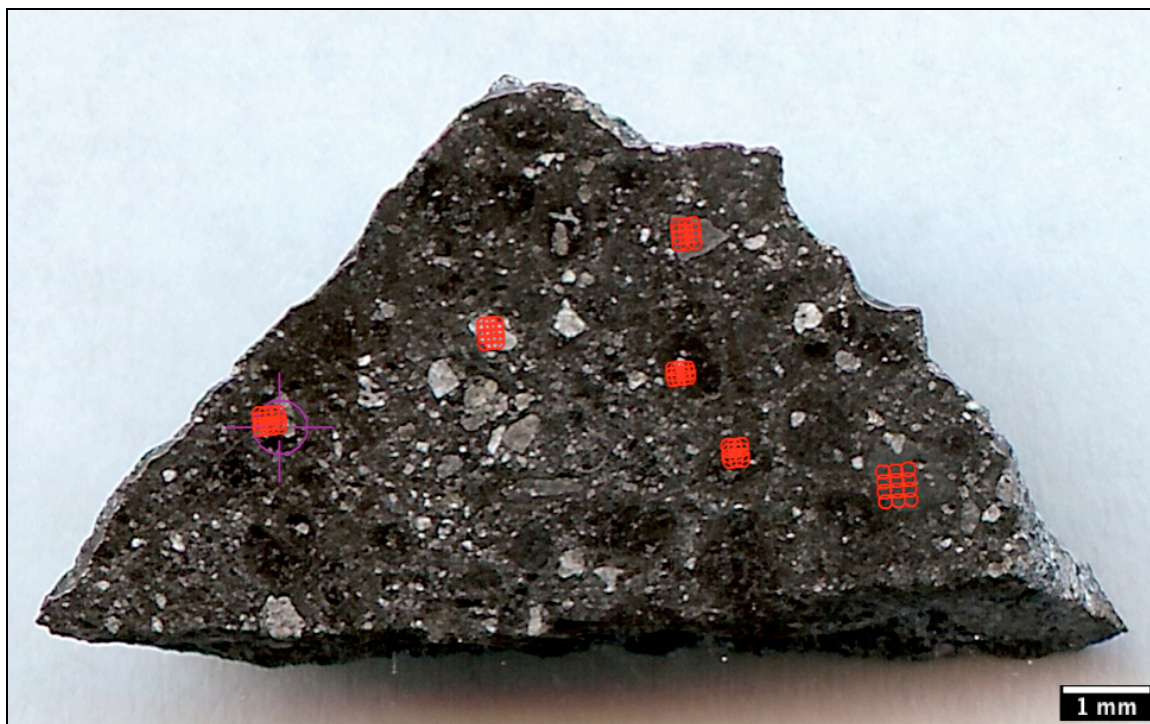


Figure 2.3 EPMA locations for NWA 7034. Each red circle represents an EPMA observation; grids of points were taken to cover the area roughly covered by a LIBS spot.

2.3 ChemCam observations The ChemCam (Chemistry and Camera) instrument onboard the Mars Science Laboratory (MSL) *Curiosity* rover uses laser-induced breakdown spectroscopy (LIBS) to quickly and remotely analyze rock and soil targets in Gale Crater, Mars (Figure 2.4).

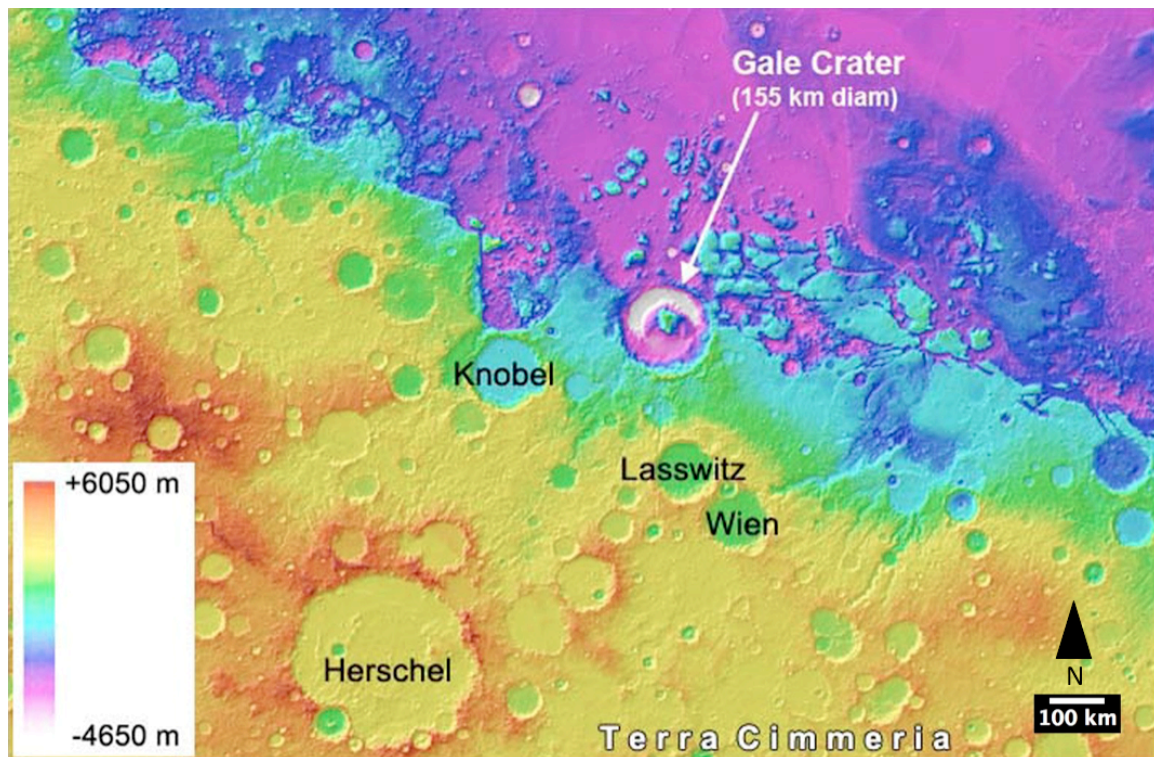


Figure 2.4 Gale crater geologic context. Gale is on the boundary of the martian dichotomy between the southern highlands and northern lowlands at 5°S, 138°E. Elevation data from Mars Orbiter Laser Altimeter (MOLA)

Within Gale, several ChemCam targets had compositions similar to NWA 7034 including Jake M (sols 45 and 48), Ashuanipi (sol 337), La Reine (sol 346), and Harrison (sol 514). Jake M is one of the first targets analyzed by ChemCam. The target is a float rock located near the MSL landing site (Figures 2.5, 2.6), and initial ChemCam and Alpha Particle X-ray Spectrometer (APXS) data show its composition to be mugearitic (Stolper et al., 2013). Both Ashuanipi and La Reine are float rocks found along the traverse from Yellowknife Bay to Mt. Sharp (Fig. 2.5). Ashuanipi is a dark-colored rock first noted for having lower Al than other targets in the area (9.7% Al_2O_3 compared to the average of 12% for the area). It has a shiny exterior coating as seen in the Remote Micro Imager (RMI) images in Figure 2.7. The target was picked to study the diversity of the

rocks in the area, so while it does not represent the immediate location in Gale crater, it would have been transported from nearby through a natural event such as an impact or an aeolian or fluvial process. La Reine is a coarse-grained rock (see Figure 2.8) with a pyroxene and feldspar composition, similar to the first ChemCam target on Mars, Coronation (sol 13, also a float rock). The ChemCam RMI and LIBS results of La Reine show analysis of a Mg-rich LIBS location as well as a feldspathic-looking location, while the rest of the sampled locations seem to be a mixture of the two end members. This suggests La Reine is a micro-gabbro, implying formation from an Fe- and Mg-rich, Si-poor magma. Both Ashuanipi and La Reine were chosen as targets to compare to NWA 7034 after a Sammon's map (Lasue et al., 2011) was created using NWA 7034 LIBS data and a selection of ChemCam targets. This process will be discussed in Section 4. Harrison is a rock composed of a gray matrix with light-toned, elongated phenocrysts about 10 mm long (Figure 2.9). ChemCam analysis shows the feldspar crystals have a significant An component and the pyroxenes trend toward pigeonite. Harrison, a possible basalt/gabbro igneous cumulate, was immediately noted as being similar to NWA 7034 in phase relation and mineral composition after being imaged during the mission.

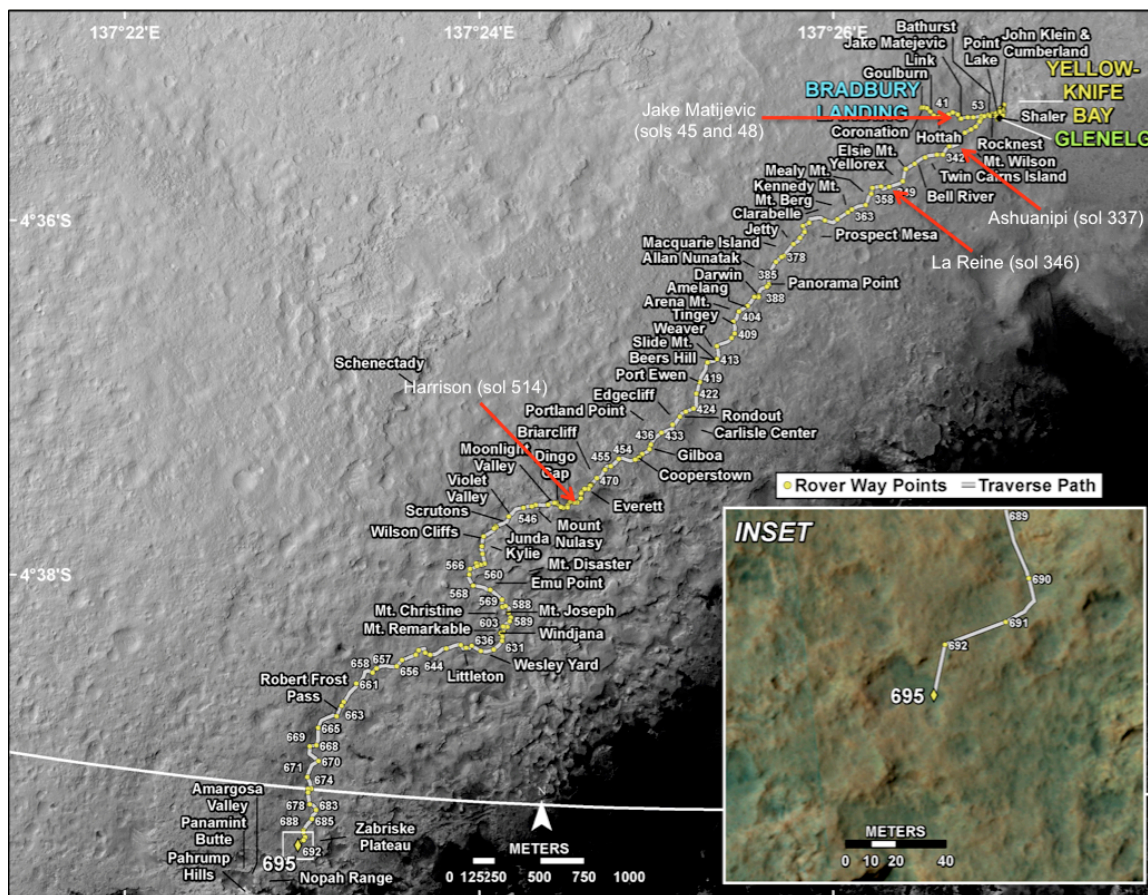


Figure 2.5 Traverse map for MSL from landing to Sol 588. ChemCam observed Jake M (labeled Jake Matije vic in the image), Ashuanipi, La Reine, and Harrison on sols 45 and 48, 337, 346, and 514, respectively. Corresponding waypoints are highlighted. Image Credit: NASA/JPL/Fred Calef.

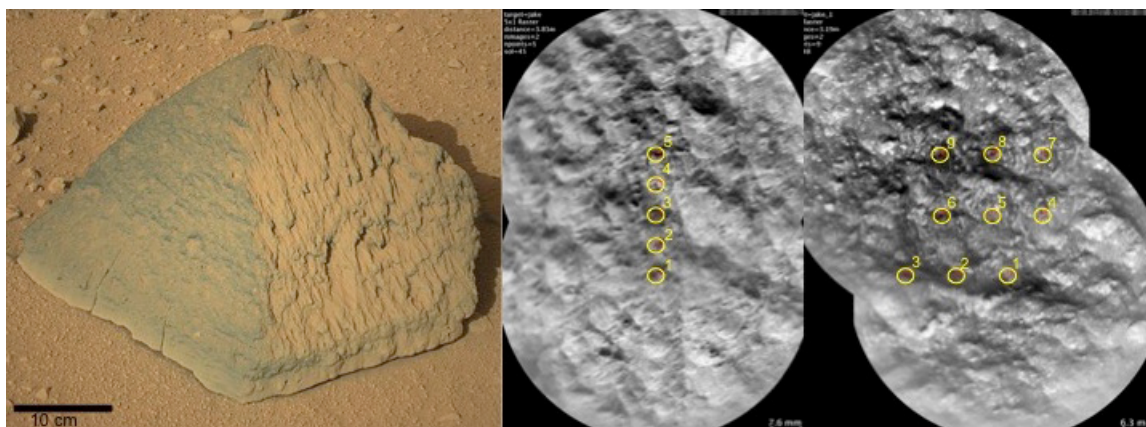


Figure 2.6 Left: MSL Mastcam image of Jake M rock. Image credit: NASA/JPL-Caltech/MSSS. **Right:** ChemCam pre- and post-LIBS RMI mosaics for sols 45 and 48. Locations in the 1x5 and 3x3 rasters are labeled. RMI image credits: NASA/JPL-Caltech/LANL.

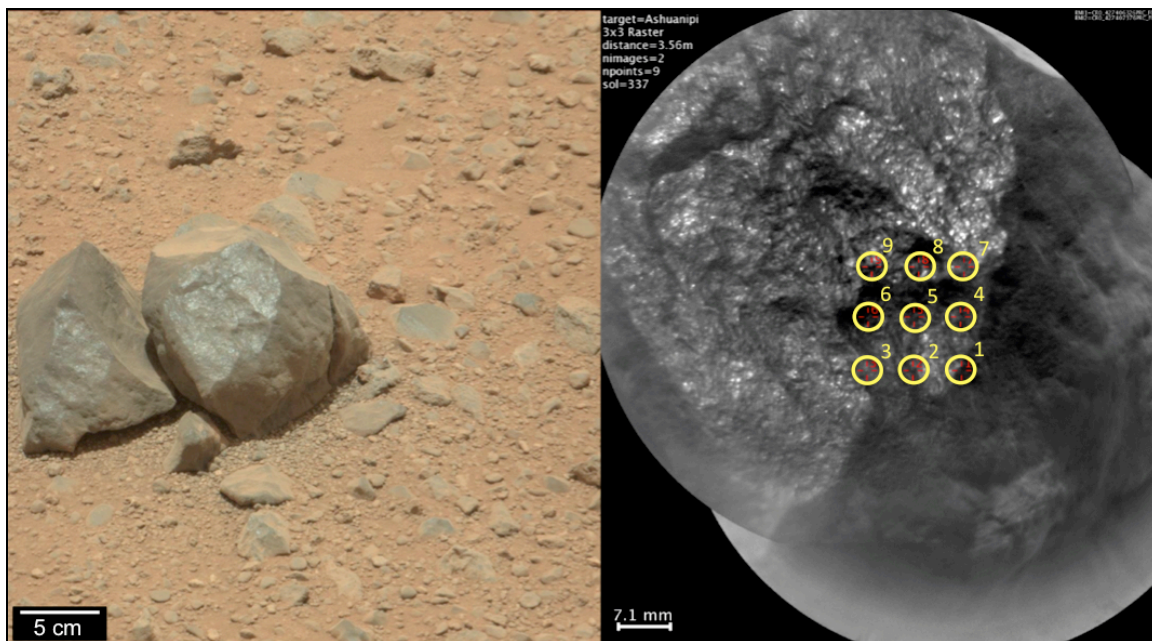


Figure 2.7 Left: MSL Mastcam image of Ashuanipi rock. Note the dark color and shiny exterior. Image credit: NASA/JPL-Caltech/MSSS. **Right:** ChemCam pre- and post-LIBS RMI mosaic. Each location in the 3x3 raster is labeled. RMI image credits: NASA/JPL-Caltech/LANL.

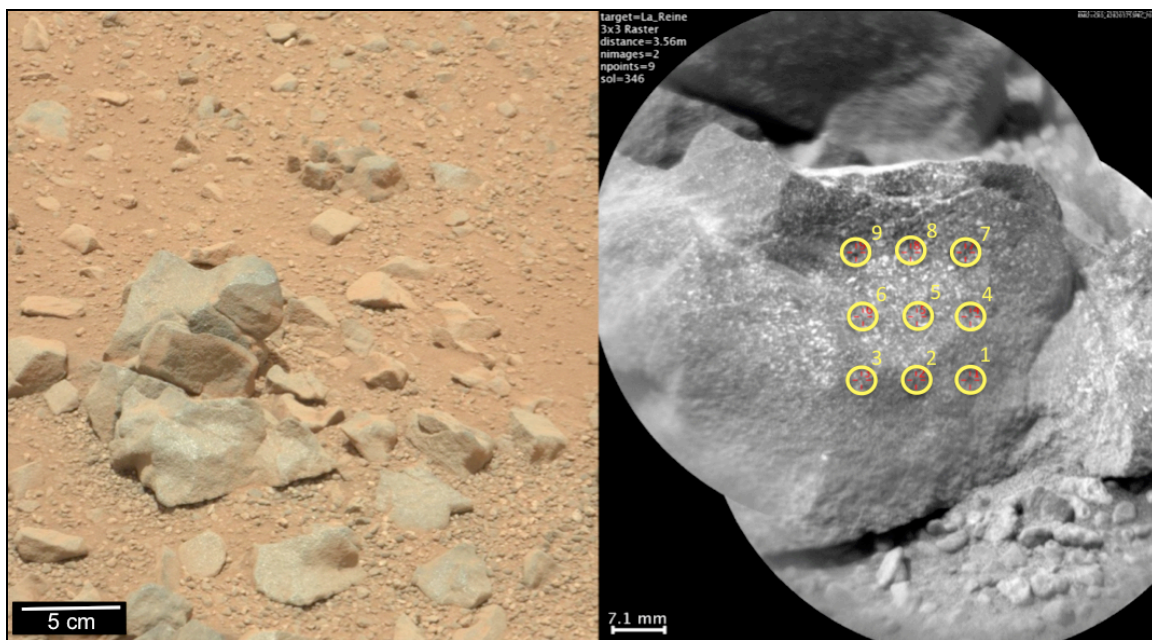


Figure 2.8 Left: MSL Mastcam image of La Reine rock. Note the mid-tone color and coarse grain size. Image credit: NASA/JPL-Caltech/MSSS. **Right:** ChemCam pre- and post-LIBS RMI mosaic. Each location in the 3x3 raster is labeled. RMI image credits: NASA/JPL-Caltech/LANL.

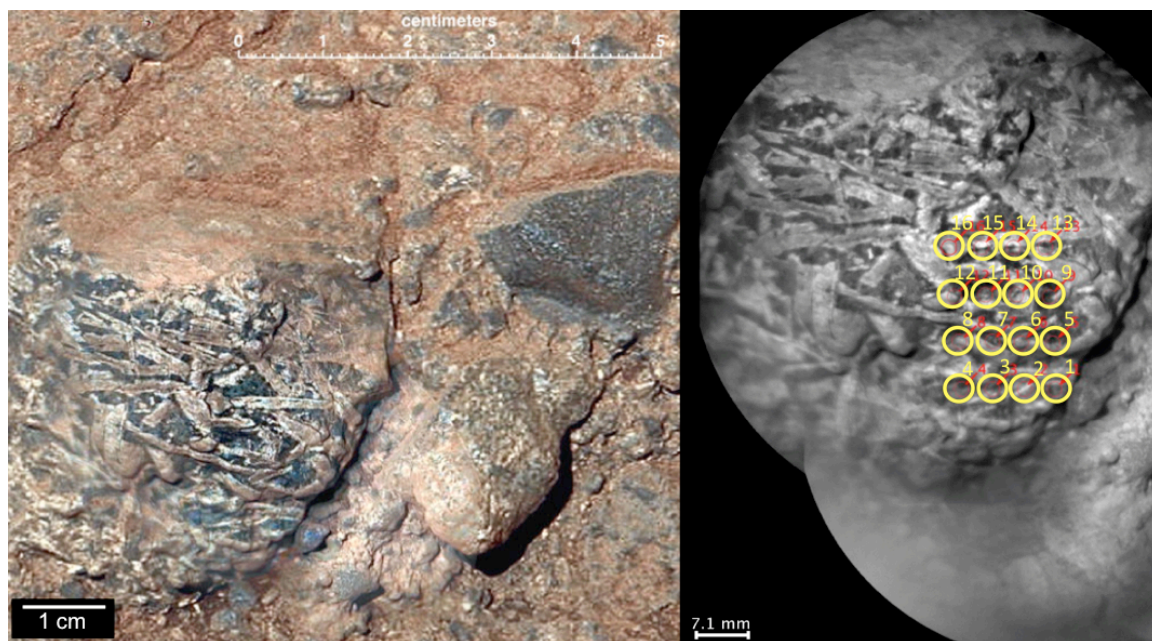


Figure 2.9 Left: MSL Mastcam image of Harrison rock. Note the dark toned matrix and elongated, light toned phenocrysts. Image credit: NASA/JPL-Caltech/MSSS. **Right:** ChemCam pre- and post-LIBS RMI mosaic. Each location in the 4x4 raster is labeled. RMI image credits: NASA/JPL-Caltech/LANL.

3. RESULTS

3.1 Summary This Partial Least Squares (PLS) analysis of SiO₂, TiO₂, FeO, and Na₂O in NWA 7034 marks the first use of the updated ChemCam calibration set (Clegg et al., 2014). The new calibration set encompasses the compositional range of NWA 7034 more completely, thus giving better oxide predictions than the old calibration set (e.g. Tucker et al., 2010). Due to the small-scale heterogeneity in the matrix of NWA 7034, all 18 spots analyzed show similar basaltic compositions. The tables in Section 3.2 show the average elemental composition of all the laser shots taken at each location.

3.2 LIBS and EPMA table summaries LIBS data are reported using the processing technique that most closely fits the EPMA bulk composition of NWA 7034 as reported by Agee et al. (2013); thus, reported data are a mix of PLS and univariate results.

	LIBS Loc.	SiO ₂	TiO ₂	Al ₂ O ₃	FeOT	MgO	CaO	Na ₂ O	K ₂ O	Total
	RMSEP	5.3	0.4	1.4*	1.9	0.5*, 1.5	1.8	0.5	0.1*	--
Round 1	1	50.8	0.8	9.4*	18.8	9.8	4.5	2.6	0.3*	97.0
	2	47.6	1.0	9.8*	17.0	9.0	7.7	2.2	0.2*	94.5
	3	52.1	0.7	9.3*	18.1	13.1	3.4	2.3	0.2*	99.2
	4	50.3	0.9	9.6*	18.6	11.2	3.7	2.5	0.2*	97.0
	5	51.0	0.8	9.8*	18.0	10.7	4.7	2.4	0.3*	97.7
	6	45.4	1.1	8.8*	17.4	8.0	9.5	2.3	0.2*	92.7
	7	54.1	0.7	10.5*	16.3	12.2	3.3	2.5	0.2*	99.8
	8	50.6	0.9	9.7*	17.8	9.3	4.5	2.6	0.2*	95.6
	9	49.9	1.0	8.6*	17.6	11.3	4.9	2.4	0.2*	95.9
	10	55.0	0.5	10.6*	15.4	12.6	3.5	2.5	0.2*	100.3
	Average	50.7	0.8	9.6*	17.5	10.7	5.0	2.4	0.2*	96.9
Round 2	1	49.2	1.1	7.8*	17.9	10.7*	4.5	2.6	0.2*	94.0
	2	47.6	1.0	7.4*	18.7	9.3*	5.5	2.4	0.4*	92.3
	3	41.3	1.4	7.5*	18.3	3.4*	10.5	2.2	0.2*	84.8
	4	47.6	0.9	8.7*	19.1	9.7*	4.5	2.5	0.3*	93.3
	5	51.6	0.8	8.6*	17.5	12.6*	4.3	2.5	0.5*	98.4
	6	47.9	1.2	6.1*	19.3	11.0*	4.7	2.6	0.5*	93.3
	7	45.3	1.2	6.8*	19.5	8.0*	6.5	2.6	0.4*	90.3
	8	51.7	0.6	9.3*	17.6	10.8*	4.2	2.7	0.5*	97.4
	Average	47.8	1.0	7.8*	18.5	9.4*	5.6	2.5	0.4*	93.0
Both	Average	49.3	0.9	8.7*	18.0	10.1	5.3	2.5	0.3*	95.0

Table 3.1 Major oxide PLS data for first and second round of LIBS locations (shown in Figures 2.7 and 2.8). Each value is an average of 150 laser pulses, except for location 1 data for the first round of LIBS values, which are averages of 50 laser pulses. Data denoted with an asterisk are univariate results.

EPMA Location	SiO₂	TiO₂	Al₂O₃	FeO	MgO	CaO	Na₂O	K₂O	Total
Location 10	53.5	0.16	8.60	13.4	17.1	4.11	1.65	0.26	99.6
Location 9	52.1	0.36	10.8	14.9	14.0	3.77	2.35	0.35	99.1
Light Toned 1	45.9	1.34	13.4	20.4	8.75	6.21	3.40	0.30	100.3
Light Toned 2	50.7	0.53	14.1	15.0	10.5	5.16	3.41	0.32	100.2
Light Toned 3	60.3	0.02	24.9	0.22	0.02	5.75	7.72	0.67	99.6
Light Toned 4	54.1	0.33	1.83	15.2	26.0	1.84	0.04	0.03	100.2

Table 3.2 EPMA data for probe locations on NWA 7034 (shown in Figure 6). Each value is the average of a grid of EPMA points (excluding those that gave totals outside the $100 \pm 2\%$ range) that roughly covers the spot size of a LIBS spot.

LIBS Location	SiO₂	TiO₂	Al₂O₃	FeO	MgO	CaO	Na₂O	K₂O	Total
<i>RMSEP</i>	7.1	0.55	3.7	4	3	3	0.7	0.9	--
Jake 1	63.9	0.35	6.9	19.8	2.5	1.7	3.5	1.5	100.2
Jake 2	50.1	2.11	9.3	21.7	2.4	6.2	1.8	0.3	93.9
Jake 3	69.0	0.42	14.2	15.3	0.3	3.3	4.1	2.0	108.6
Jake 4	54.5	0.61	10.9	14.2	2.6	5.0	3.0	1.4	92.2
Jake 5	48.4	1.05	9.0	15.0	3.8	8.5	2.9	0.9	89.6
Jake_1 1	63.6	0.62	11.7	13.6	1.5	6.5	4.4	1.9	103.9
Jake_1 2	55.0	1.59	10.1	19.6	1.3	6.0	2.6	1.1	97.3
Jake_1 3	60.2	0.86	11.4	15.4	0.4	5.5	3.2	1.8	98.8
Jake_1 4	46.0	0.83	8.0	14.9	3.1	9.2	2.8	0.8	85.6
Jake_1 5	67.6	0.0	12.8	9.8	0.0	3.0	5.6	3.0	101.8
Jake_1 6	58.1	1.35	9.8	19.4	1.6	7.4	2.9	0.9	101.5
Jake_1 7	59.2	0.95	10.5	18.0	0.7	6.4	3.5	1.7	101.0
Jake_1 8	53.1	1.18	9.0	16.2	2.0	8.1	3.0	0.8	93.4
Jake_1 9	49.9	0.98	6.9	15.7	5.9	14.6	2.6	0.7	97.3

Table 3.3 Major oxide data for Jake M (shown in Figure 2.6). Each value is an average of 30 laser pulses.

LIBS Location	SiO₂	TiO₂	Al₂O₃	FeOT	MgO	CaO	Na₂O	K₂O	Total
<i>RMSEP</i>	7.1	0.55	3.70	4.0	3.0	3.0	0.7	0.9	--
Ashuanipi 1	52.9	0.73	8.10	16.5	9.1	6.6	3.0	1.2	98.1
Ashuanipi 2	42.5	0.89	4.8	16.9	12.1	9.8	1.5	0.0	88.6
Ashuanipi 3	51.0	0.81	8.50	16.2	11.7	6.4	2.3	0.7	97.7
Ashuanipi 4	49.6	3.08	14.0	16.0	9.0	6.8	2.6	1.3	102.4
Ashuanipi 5	55.4	0.61	9.40	14.9	9.1	6.2	3.3	1.4	100.4
Ashuanipi 6	57.4	1.33	15.6	12.9	4.4	6.5	4.3	1.3	103.8
Ashuanipi 7	50.2	1.09	9.30	15.6	11.4	7.8	2.1	0.6	98.1
Ashuanipi 8	51.5	1.11	7.70	15.5	11.5	6.2	2.4	1.6	97.5
Ashuanipi 9	52.6	1.80	9.50	16.2	12.6	6.7	2.2	1.3	102.9
<i>Average</i>	51.5	1.30	9.70	15.6	10.1	7.0	2.6	1.0	98.8

Table 3.4 Major oxide data for Ashuanipi (shown in Figure 2.7). Each value is an average of 30 laser pulses.

LIBS Location	SiO₂	TiO₂	Al₂O₃	FeOT	MgO	CaO	Na₂O	K₂O	Total
<i>RMSEP</i>	7.1	0.55	3.7	4.0	3.0	3.0	0.7	0.9	10.0
La Reine 1	58.3	1.47	10.3	15.4	10.6	6.9	2.6	0.5	106.1
La Reine 2	53.6	1.35	8.3	16.2	13.3	7.7	2.0	0.5	102.8
La Reine 3	58.8	1.09	13.0	15.2	9.4	7.5	3.3	0.9	109.2
La Reine 4	50.5	2.06	9.9	15.1	12.0	7.1	2.1	0.5	99.2
La Reine 5	55.6	0.88	8.4	15.2	11.4	5.9	2.8	0.7	101.0
La Reine 6	50.0	1.57	7.7	16.4	14.2	6.2	2.1	0.6	98.8
La Reine 7	57.4	0.86	10.0	15.8	8.7	7.9	3.0	0.3	103.9
La Reine 8	50.7	0.98	5.1	18.2	15.4	5.6	1.2	-0.2	97.1
La Reine 9	51.1	1.72	10.3	16.5	11.2	9.1	2.3	0.4	102.6
<i>Average</i>	50.4	1.30	9.20	16.0	11.8	7.1	2.4	0.5	102.3

Table 3.5 Major oxide data for La Reine (shown in Figure 2.8). Each value is an average of 30 laser pulses.

LIBS Location	SiO₂	TiO₂	Al₂O₃	FeOT	MgO	CaO	Na₂O	K₂O	Total
RMSEP	7.1	0.55	3.7	4.0	3.0	3.0	0.7	0.9	10.0
Harrison 1	48.3	1.54	9.70	13.2	2.30	11.4	2.20	1.50	90.2
Harrison 2	43.8	1.17	9.90	7.30	5.20	10.7	2.30	2.30	82.7
Harrison 3	47.6	0.60	12.5	8.70	0.00	-0.30	1.90	2.30	73.3
Harrison 4	36.2	1.21	8.40	6.60	4.20	19.0	2.10	1.60	79.4
Harrison 5	41.7	1.13	3.60	9.50	0.20	4.60	1.20	0.00	62.0
Harrison 6	44.1	0.42	12.0	11.5	-2.10	0.80	1.50	1.40	69.5
Harrison 7	52.9	0.98	12.6	14.5	-0.90	5.20	2.20	1.20	88.6
Harrison 8	46.3	0.46	11.6	9.60	-0.70	1.40	1.40	2.60	72.7
Harrison 9	39.5	1.43	4.80	14.6	5.90	19.5	1.30	0.50	87.5
Harrison 10	44.4	1.98	10.3	16.4	2.10	10.4	1.70	1.20	88.5
Harrison 11	46.2	1.25	11.5	11.8	1.00	9.40	1.80	2.60	85.6
Harrison 12	58.4	0.61	13.4	6.00	5.10	1.90	3.30	1.30	90.0
Harrison 13	48.1	0.95	11.6	14.2	-0.90	3.80	1.70	1.90	81.3
Harrison 14	62.5	0.55	14.3	6.00	3.20	5.00	4.50	1.50	97.5
Harrison 15	61.5	0.61	13.2	5.50	4.30	2.50	4.30	1.40	93.3
Harrison 16	59.0	0.82	14.7	5.90	4.80	3.70	3.60	0.90	93.4
Average	48.8	1.00	10.9	10.1	2.10	6.80	2.30	1.50	83.5

Table 3.6 Major oxide data for Harrison (shown in Figure 2.9). Each value is an average of 30 laser pulses.

4. DISCUSSION

4.1 NWA 7034 LIBS results interpretation The results of the two rounds of LIBS observations performed on NWA 7034 can be discussed in terms of bulk, location-based, or shot-to-shot compositions. Beginning with a bulk analysis, the average of all LIBS spectra taken on the meteorite gives a composition in the basalt region. To put the NWA 7034 measurements in the perspective of the whole martian data set, the LIBS data from this study and the EPMA bulk data from Agee et al. (2013) were plotted on a total alkali versus silica (TAS) diagram shown in Figure 4.1. The blue and purple squares, representing NWA 7034 EPMA and LIBS bulk compositions, agree within error on the SiO_2 axis but do not overlap on the $\text{Na}_2\text{O} + \text{K}_2\text{O}$ axis. This is reflected in the tabulated data, showing the LIBS totals with lower overall alkalis and similar SiO_2 percentages. The MER APXS bulk composition, EPMA bulk composition of NWA 7034 from Agee et al. (2013), and LIBS bulk composition of NWA 7034 from this study all plot within the basalt field of the TAS diagram with single sample outliers spanning the entire range of SiO_2 values and into the trachybasalt/tephrite field in alkali abundance. The bulk composition of NWA 7034 by LIBS reported in this study is just outside the error of the bulk reported by Agee et al. (2013), although both compositions plot in the basalt field. It should be noted that the bulk composition reported by Agee et al. (2013) might not be representative of the bulk composition of the sample used in this study due to the heterogeneity of the meteorite. The similarity of NWA 7034 to MER basalts has been pointed out by many authors (e.g. Agee et al., 2013), but comparison with MSL APXS data has not been explored until now. While the bulk MSL APXS value plots outside of

the basaltic range, the SiO₂ error bars overlap with the error bars of the MER and NWA 7034 EPMA bulk compositions. Further comparison of NWA 7034 and MSL LIBS data is included in section 4.4. The LIBS data plot at lower alkali values as compared to the EPMA data for NWA 7034 and the rest of the martian data plotted on the diagram. Because K and Na are volatile elements, one possible explanation for the lower totals in LIBS data could be that these two elements were volatilized during analysis. However, this is probably not the case because the discrepancy is most likely due to poor quantification of Na due to its dominant emission peaks in the VNIR range of the LIBS spectra, at 589 and 819 nm. When LIBS spectra are normalized to the intensity of each spectrometer (so that the total intensity sums to 3), the Na peak is much larger than any other peak in the spectrum. At the same time, the standards used for univariate data analysis have a small range of Na values with which to compute calibration curves for the element. This leads to underestimated Na predictions, as reported by Fabre et al (2014).

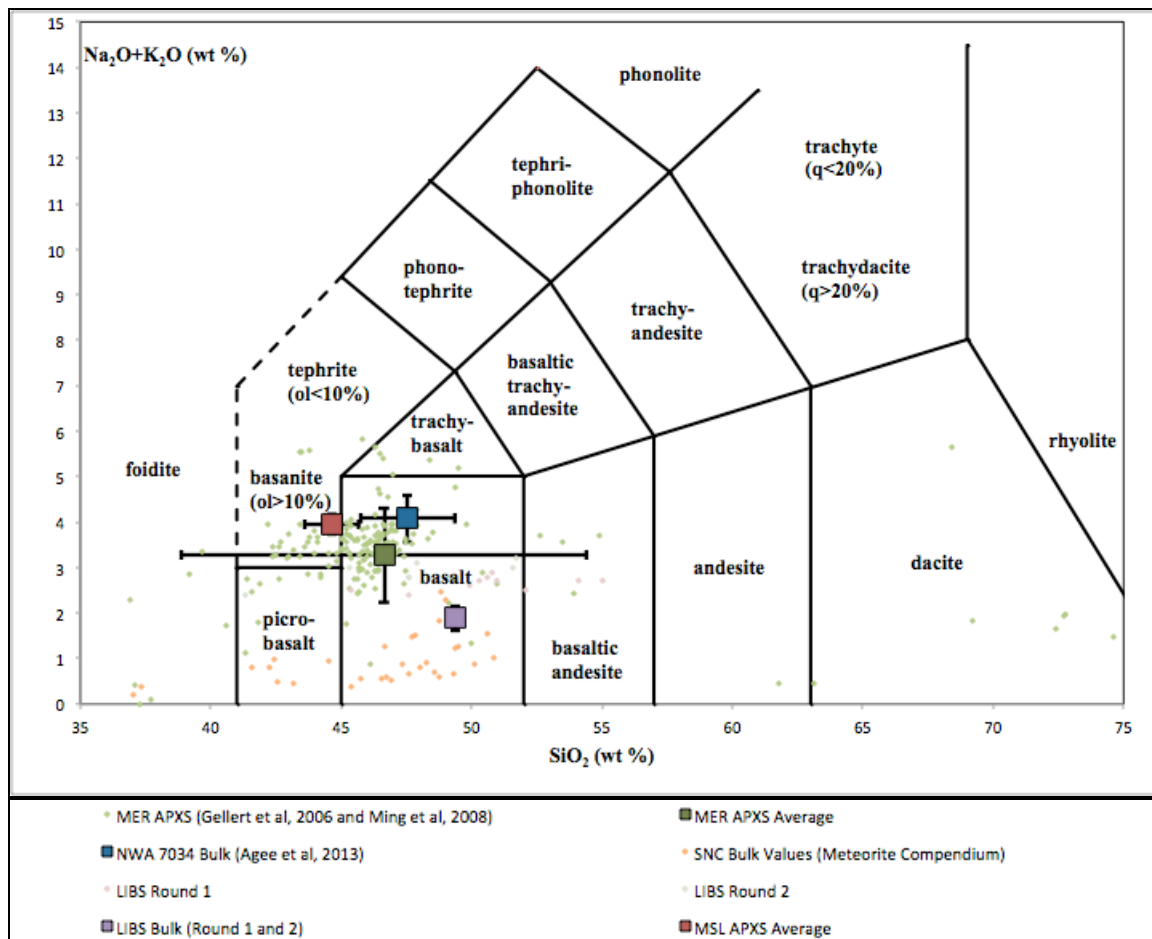


Figure 4.1 This total alkali versus silica (TAS) diagram shows a comparison of Mars data from MER APXS mission data, SNC bulk values, MSL APXS mission data, and NWA7034 LIBS and EPMA measurements. For the LIBS Round 1 and Round 2 data, each point represents an average of 150 spectra for each observation location. The large squares with error bars are the average of their respective datasets, while smaller points represent the bulk composition of single samples.

While it can be useful to look only at bulk data for certain samples, it has been noted (e.g. Wiens et al., 2002) that LIBS analyses on heterogeneous samples like NWA 7034 will give less-than-desirable bulk results. It can be argued that a bulk composition is not necessary to understand the individual components of this unique sample, as is the goal of this study. On a location-to-location level, the best way to test the ability of LIBS to determine different rock types is by comparing different clasts within the meteorite.

The most thoroughly analyzed clasts in this study are labeled as Locations 9 and 10 in the LIBS Round 1 image (Figure 2.1). Location 8 in the LIBS Round 2 image (Figure 2.2) is the same clast as Round 1 Location 10. EPMA data were also acquired on these clasts as seen in Figure 2.3, and are discussed in Section 4.2. Backscatter electron (BSE) images of the clasts are shown in Figure 4.2. The insets in Figure 4.2C and 4.2E show the small-scale heterogeneity of the clasts, with a bigger variety in grain size in Location 9. Each clast contains various pyroxenes, plagioclase, Cl-rich apatite, ilmenite, and Cr-rich magnetite; however, the two clasts have different abundances of those minerals. Because the LIBS analysis points are located entirely within each clast, analysis of shot-to-shot data should indicate different compositions for these two clasts. Figure 4.3 shows a comparison of Round 1 LIBS data for Locations 9 and 10. The shot-to-shot data plot in separate clusters for each clast, and the average compositions of each clast plot within their respective clusters. The clast observed at Location 9 (Figure 4.2A-C and the blue data points in Figure 4.3) shows a higher $(\text{Fe}+\text{Mg})/\text{Si}$ value than the clast observed at Location 10 (Figure 4.2D-F and the red data points in Figure 4.3). This difference in composition can be explained by the higher amount of Fe-rich oxides in the Location 9 clast (Figure 4.2C), and it could also possibly be due to a higher Ca content in the pyroxene grains found in Location 9.

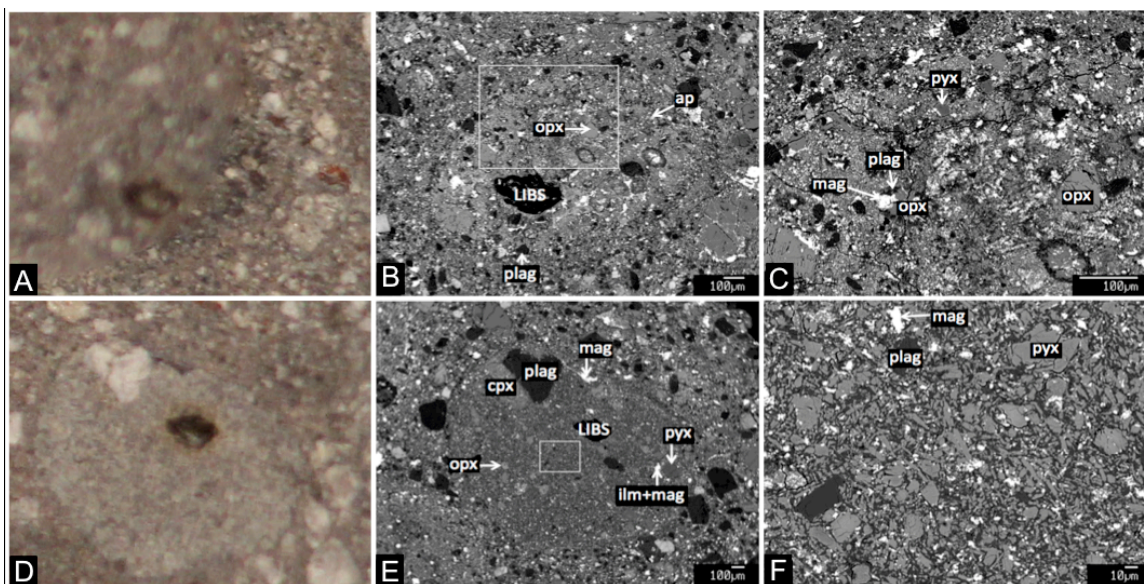


Figure 4.2 Optical and Backscattered Electron (BSE) images of clasts that include LIBS Locations 9 (A,B,C) and 10 (D,E,F). Insets shown in B and E are magnified in C and F, respectively. Label definitions: LIBS = LIBS pit, opx = low-Ca pyroxene, cpx = high-Ca pyroxene, pyx = pyroxene, plag = plagioclase, ap = Cl-rich apatite, ilm = ilmenite, mag = Cr-rich magnetite.

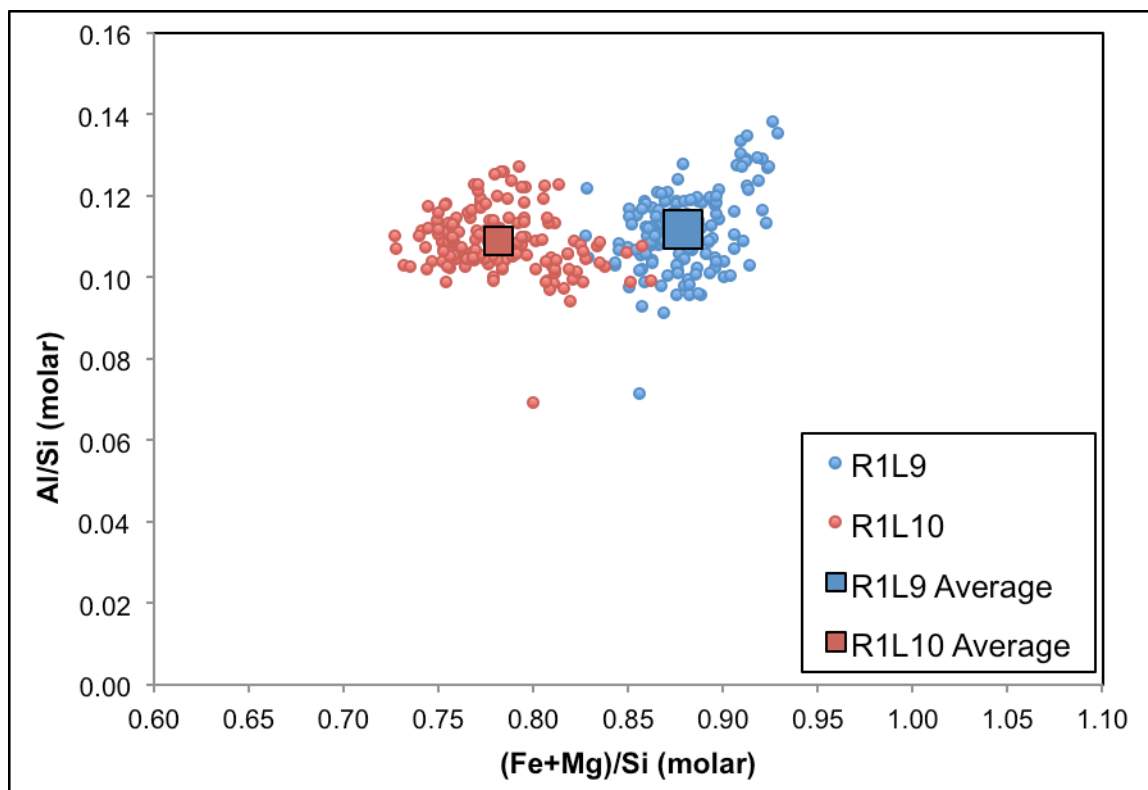


Figure 4.3 Clast comparison of Locations 9 and 10 for round 1 of LIBS. Plot of shot-to-shot data shows barely any overlap between clasts, with similar Al/Si values but distinct (Fe+Mg)/Si compositions. Standard deviation of the mean for each location is equal in size to the squares representing each location's average composition.

Because the RMSEP error bars are calculated based on the method of multivariate analysis and not on the values of the laser shots themselves, further statistical verification of the uniqueness of both clasts was performed. Before any statistical tests on the data, it was confirmed that each LIBS location's shot-to-shot data approximated a normal distribution by binning and plotting the data in histograms (Figure 4.4) and plotting the full data set on a normal probability plot (Figure 4.5). Another measure of statistical significance is the standard deviation of the mean, calculated as the standard deviation divided by the square root of the number of observations. For these two clasts, the standard deviation is below 0.001 on the Al/Si axis and below 0.05 on the (Fe+Mg)/Si

axis. These values divided by the square root of 150 shots give error bars represented by the size of the squares marking the average compositions for the clasts.

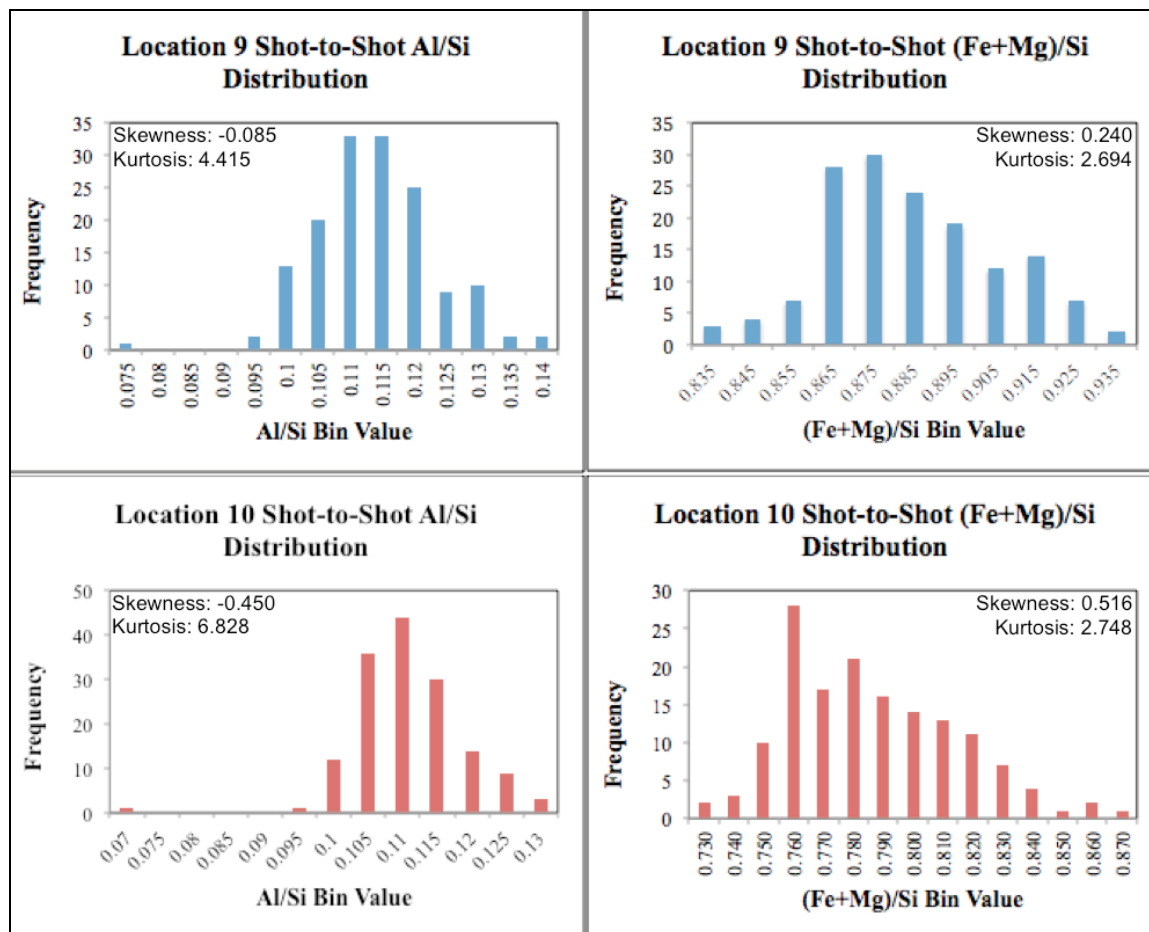


Figure 4.4 Frequency distribution of shot-to-shot LIBS analyses on Round 1, Locations 9 and 10 showing a Gaussian distribution for both Al/Si and (Fe+Mg)/Si ratios.

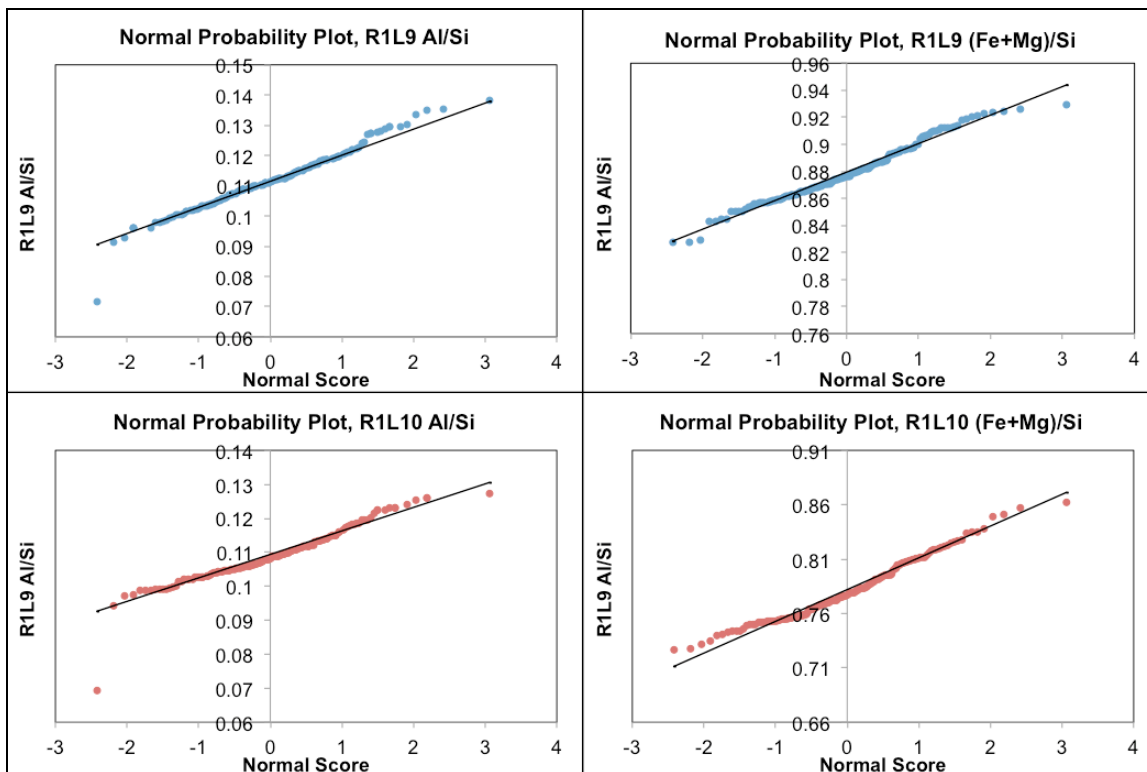


Figure 4.5 Normal probability plots for Al/Si and (Fe+Mg)/Si data for LIBS Round 1, Locations 9 and 10. The solid black line represents the normal scores for a perfectly normal distribution, and the colored points are the real data, showing little variation from a normal distribution.

The distribution and separation of the two clasts shown here exemplifies the repeatability of LIBS analyses, but the calibration dataset for the PLS and univariate analyses greatly affects the accuracy of reported oxide totals. Work is ongoing to ensure all PLS and univariate analyses are accurate as well as precise, allowing LIBS not only to distinguish between compositions in heterogeneous samples, but also to lend insight to the formation histories and regional origins of martian samples. The ability of LIBS instrumentation to distinguish between the two clasts in LIBS Round 1 has important implications for martian ChemCam observations. Even if clasts in a ChemCam target have similar mineralogy, comparison of each LIBS location should reveal when two

separate clasts are observed. The RMI images of the target can then be checked to ensure the LIBS locations were entirely inside the clasts.

Looking further into the location-based and shot-to-shot LIBS results, the unique compositions included in NWA 7034, both on the sample surface and at depth, can be determined on a ~350 micron scale. To perform a depth profile at a certain LIBS location, the spectra taken at each laser pulse can be examined either qualitatively or quantitatively. In this study, a qualitative depth study was performed on a clast of NWA 7034 that was hit by 150 laser pulses during the first round of LIBS analyses. Comparison of some of the first and last spectra produced through observation of this clast, labeled Location 10 in Figure 2.1, shows how the distribution of elements and minerals changes with the ablation of sample volume after each laser pulse. Due to the hardness of the meteorite, each pulse ablated about 0.3 microns giving a total LIBS pit depth of about 45 microns. Standard procedure for ChemCam LIBS analysis is to remove the first five laser pulses from every location sampled, allowing for removal of any interfering dust on the surface. Although this sample was not dust-covered in the lab, the first 5 shots will still be disregarded. The spectra at either end of the observation can be compared by creating a difference spectrum. Figure 4.6 shows an example of a difference spectrum, created by normalizing the average spectral intensities of one location on each of two selected targets into z-scores as follows:

$$Z_n = \frac{(i_n - \bar{i})}{\sigma} \quad (4.2)$$

where i_n is the intensity at a given wavelength, \bar{i} is the mean intensity of every wavelength for that observation, and σ is the standard deviation for that observation. The difference between the two observations' z-scores is then plotted as a spectrum. The z-

scores calculate the distance from the mean intensity of the observation in terms of standard deviations. This normalizes the intensities from the two separate observations and makes them comparable in a difference spectrum. The values plotted in the figure represent the z-score of the first shot minus the last shot at each recorded wavelength in the spectrometers. Values above zero indicate the weight percent in the first shot for the given element is higher than in the last shot. The opposite is true for the negative values in the plot. The difference spectrum shown in Figure 4.6 shows very little variation between the 6th and 150th laser shot at Location 10 in the Round 1 LIBS observation, with most of the variation coming from calcium, sodium, and magnesium and a small influence from aluminum and potassium. This indicates that as the laser shots progressed into the depth of the meteorite, the changing feldspar composition may have been the dominant source of changes in the LIBS signal intensity. The z-score plot highlights the statistical independence of shot 6 and shot 150 in this LIBS observation location, although the independence between consecutive laser shots is ambiguous. Analysis of bulk, location-to-location, and shot-to-shot LIBS data is effective at determining the general composition of NWA 7034 and other targets, as well as compositional changes with depth and unique clasts included in the sample.

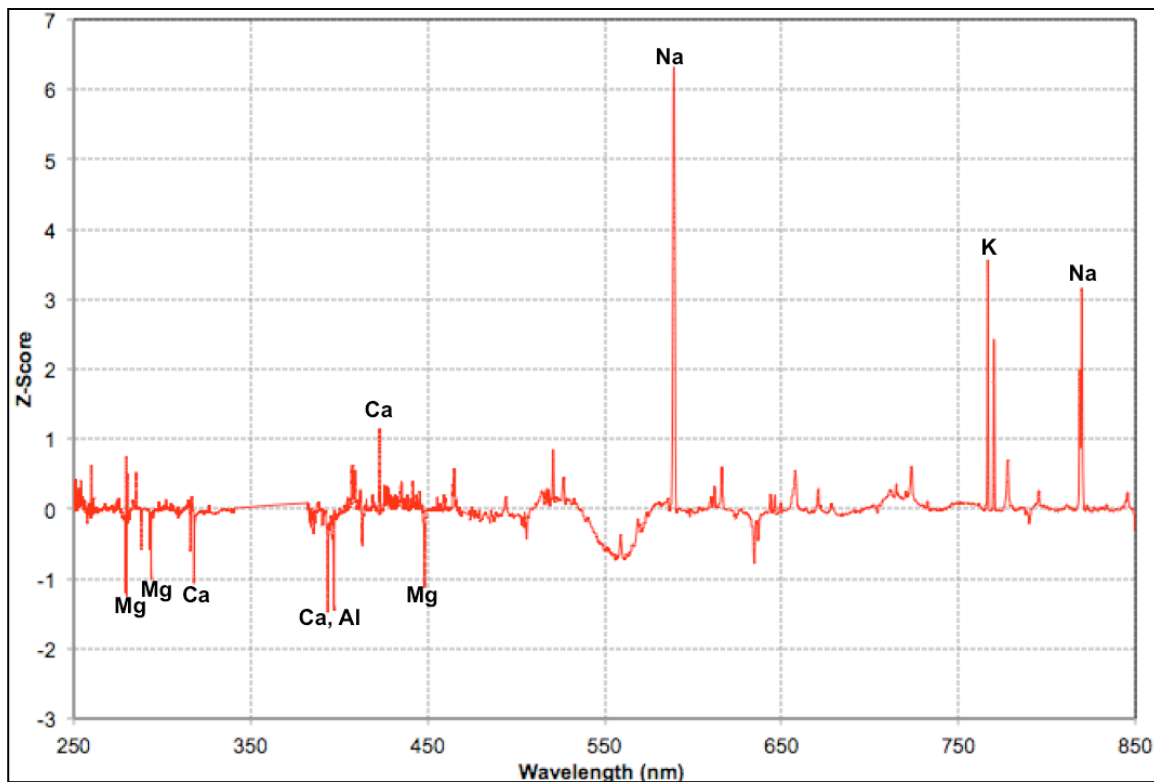


Figure 4.6 Z-score difference spectrum comparison of LIBS Round 1, Location 10, shot 6 minus shot 150. Z-score calculation is discussed above. Most of the variation is from Mg, Ca, Al, Na, and K.

4.2 Comparison of NWA 7034 LIBS and EPMA results EPMA analysis of LIBS Round 1 Locations 9 and 10 (2.9) showed similar basaltic compositions within the errors of both instruments as plotted on an Al/Si vs. (Fe+Mg)/Si graph (Figure 4.7). The same graph is used in Sautter et al. (2014) to compare ChemCam targets with NWA 7034's paired meteorite, NWA 7533. For both LIBS locations from this study, The LIBS data for Location 9 and the EPMA data for location 10 plot on the more (Fe+Mg)-rich end of the plot, while Location 9 EPMA data are more Al-rich and Location 10 EPMA data are less Al-rich than their LIBS counterparts. Comparison of the bulk composition of first 10 LIBS locations with the bulk composition of NWA 7034 given by Agee et al. (2013)

shows slight differences. These discrepancies are due to multiple factors, including the different spot sizes used in EPMA and LIBS analyses. A CIPW norm of the bulk average LIBS composition gives approximately 41% feldspar, 33% pigeonite, and 10% olivine. Comparing this to a CIPW norm computed using the average oxide compositions of microprobe analyses reported by Agee et al. (2013) of approximately 45% feldspar, 27% pigeonite, and 19% olivine, we see a similar result to the LIBS norm, keeping in mind the limited number of LIBS observations on the coarse-grained matrix.

A quantitative comparison of NWA 7034 measurements from different sources can also be seen in Figure 4.7. The LIBS bulk and clast data cluster in a lower-alkali and higher-silica region of the plot than the EPMA bulk given by Agee et al. (2013). The EPMA data from this study have similar silica values within error of the LIBS locations; however, the microprobe clast data show higher alkali concentrations. As a comparison to the basaltic, basaltic andesite, and trachyandesite clast types defined by Santos et al. (2015), the EPMA data for the clasts in LIBS Locations 9 and 10 seem to fit into the basaltic category. All the LIBS data points plot in the same location even though they compositionally do not match up with other NWA 7034 measurements, showcasing the repeatability of the LIBS observations versus to accuracy of the processed data. The precision of the instrument is inherent in the instrument (e.g. Maurice et al., 2012) while the accuracy depends on the analysis of the LIBS data. The variety and quantity of calibration samples for both PLS and univariate analysis directly affects the accuracy of the resulting elemental data.

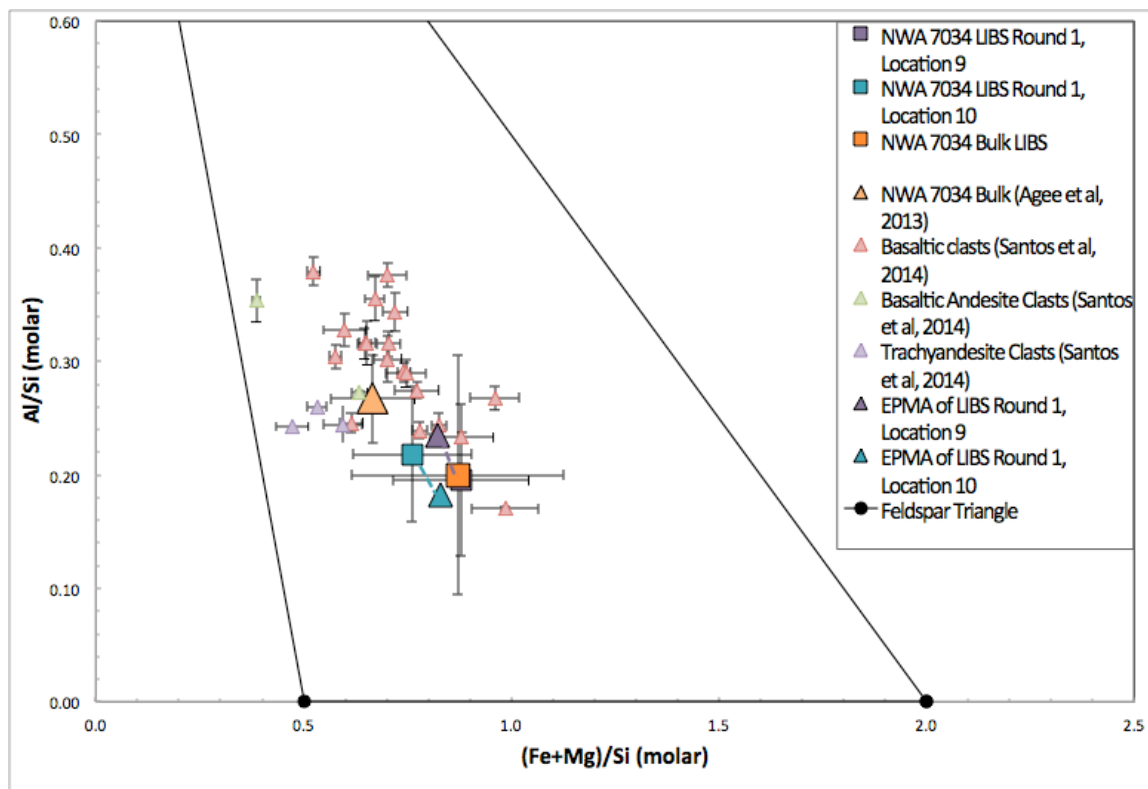


Figure 4.7 Al/Si vs. (Fe+Mg)/Si plot of NWA 7034 measurements from various sources. Triangular points are from different studies, while square- and diamond-shaped points represent the LIBS and EPMA data taken in this study. Error bars for LIBS data are calculated by propagating RMSEP values. Error bars for EPMA data are calculated by propagating univariate errors.

4.3 LIBS sampling study The ChemCam LIBS spot size (~350-500 μm depending on standoff distance) is small enough to be able to sample specific phenocrysts and clasts, but it also samples the aggregate of fine grains that are significantly smaller than the spot size. McCanta et al. (2013) created a LIBS sampling model in which they studied the importance of grain size, spot size, mineralogy, and sampling density in returning accurate bulk sample analyses. Their program, LIBSSIM (available for free at <http://www.mtholyoke.edu/~pdobosh/libssim/>), allows users to input values for all the variables mentioned above and then create and sample a randomly-built “rock” whose

mineralogy is determined by pixel values in a two-dimensional 1000x1000 pixel grid. The authors concluded that the grain size to spot size ratio was the most important factor in the reproducibility of results and that a grain size to spot size ratio of 0.25 gave both accurate and precise major element oxide totals. They also reported that a LIBS observation with ten analysis locations gave an accurate bulk rock composition when the spot size was larger than the grain size, but an average of 30-60 analysis locations were needed for a reproducible bulk rock composition when the beam size was significantly smaller than the grain size. The program used by McCanta et al. has uniform grain sizes and a two-dimensional sample space, whereas LIBS observations of heterogeneous samples are not uniform or two-dimensional. Martian meteorite NWA 7034 provides a perfect sampling study with its heterogeneous composition and varying grain sizes. Here, a semi-quantitative approach is taken using element maps of the meteorite to analyze changes in composition on the LIBS spot size scale and to determine how many analyses are needed to distinguish between matrix and clast materials.

The LIBS spot size is about 350 microns at 1.5 m standoff (so ~350 μm per “pixel”), while the element maps obtained with EDS are much higher resolution. This means the EDS images had to be reduced in resolution to find the average pixel intensity across an area on the LIBS spot size scale. Beginning with the meteorite matrix, the area of the sample surrounding LIBS Round 1, Location 2 was analyzed for pixel intensity (Figure 4.9). A 7x9 grid was created to simulate the area ablated by the LIBS analysis. Each area in the grid is 28x21 pixels, with each area in the grid corresponding to a theoretical LIBS analysis area about 350x260 microns. The areas were placed side by side to create 63 LIBS-sized analysis areas in the grid. Si, Mg, and Na element maps

were overlain with the grid, and each area's average, minimum, and maximum pixel intensities were measured. The values were then converted to a color scale and superimposed on the EDS image to show potential element intensity changes on the scale of the LIBS spot (Figure 4.9). This close spacing is unreasonable for actual LIBS analyses, which would not be immediately adjacent to one another; this model allows for an exploration of how the composition obtained in the LIBS Round 1, Location 2 analysis might change had the LIBS observation sampled a slightly different location on the meteorite matrix.

While the elemental abundances cannot be calculated directly from the pixel intensity, it is clear that Si and Mg are more abundant in the matrix than Na as seen by the overall brightness and clarity of each image. For Si, the average pixel intensity of the entire grid is 76.1 ± 3.9 (units of intensity given arbitrarily by ImageJ), not including the four grid areas that analyzed part of the LIBS spot (seen in Figure 4.9C as the two gray rectangles and the two rectangles directly below them in 4.9F and 4.9I). However, the Si pixel intensity on the LIBS spot size scale ranges from 69.9 to 85.0, well outside $2\text{-}\sigma$ of the average value. Although this is only semi-quantitative, it is helpful to see how these changes could affect the overall composition reported by LIBS analysis. As an exercise, the percent change from the lowest to highest pixel intensity inside the grid outlined in Figure 4.9(B,E,H) can be applied to the LIBS Si value given by this location. The percent difference in pixel intensity is 19.5%. There is not a qualitative correlation between the change in pixel intensity and the change in Si composition; however, this qualitative study shows that the Si value sampled by this LIBS location could have been higher or lower if the laser had hit the matrix in a slightly different location. This compositional

change, even if it is small, could affect the resulting Si composition measurement given by LIBS PLS enough to change the classification of the rock's matrix by changing its location on a Total Alkali vs. Silica (TAS) diagram, because even small changes in Si composition could change the rock type inferred from the data plotted on the diagram.

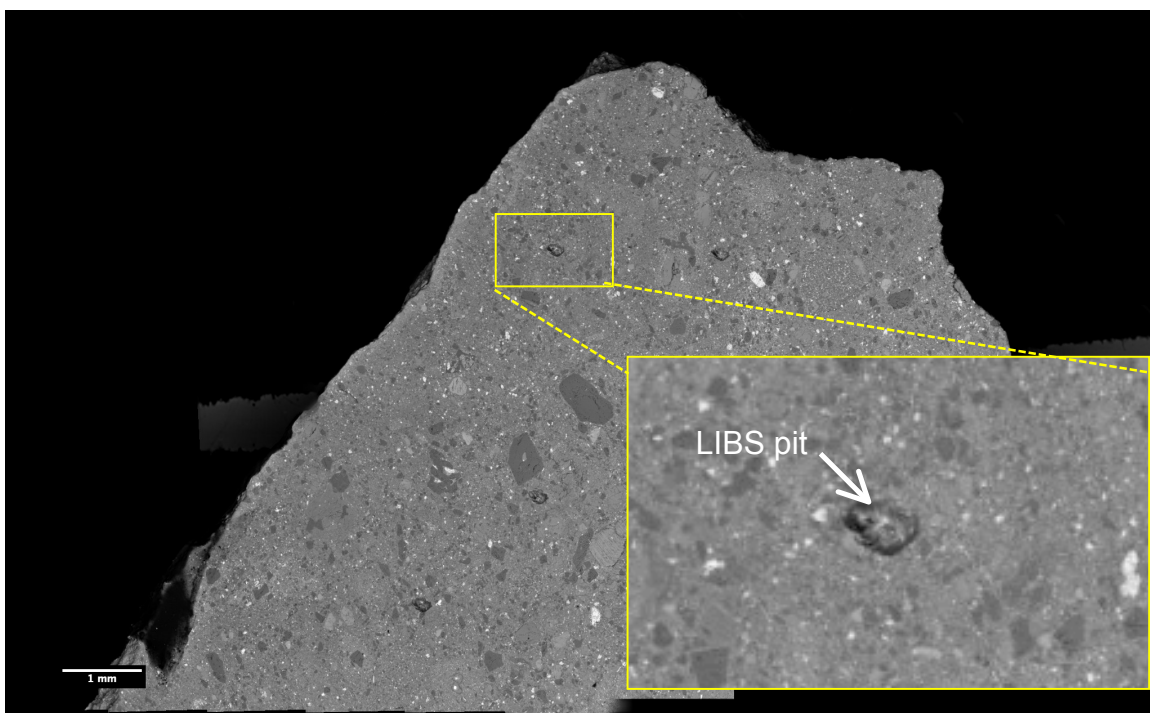


Figure 4.8 Backscattered Electron (BSE) image created after the first round of LIBS on the NWA 7034 sample. The LIBS sampling location for Round 1, Location 2 is visible in the center of the inset. This area was used in the EDS element map to calculate change in pixel intensity for Si, Mg, Na, Al, and Ca on the LIBS spot size scale.

Repeating this exercise with Mg, we see an average pixel intensity of 19.5 ± 2.6 , again excluding the LIBS spot in the image. This pixel intensity value is much smaller than the intensity value for Si, which is expected based on the relative abundances of Mg and Si in the sample. However, the percent difference between the lowest and highest Mg

values is much larger than the difference between the lowest and highest Si values at 69.6%. This is expected based on the area of analysis shown in Figure 4.9; there are both Mg-rich clasts as well as Mg-poor areas, while the Si values are more homogenous in the same region. Had the LIBS spot hit one of the areas of high Mg, it is possible that the modeled Mg composition of that location may have been much higher or lower than reported. For Na (Figure 4.9H), the total pixel intensities are much lower than for Si and Mg. The average pixel intensity for this grid is 14.1 ± 2.3 with a difference between the highest and lowest pixel values of 76.2%. As with Mg, Na varies greatly based on clast type and so the modeled LIBS composition can be vastly different depending on where the LIBS analysis point is located.

Using the grid and intensity values from Figure 4.9, a statistical analysis was performed to study the number of LIBS analysis locations needed to match the bulk pixel intensity for Si, Mg, and Na. For this exercise, random grid areas were chosen starting with groups of two areas and adding one area at a time until their average pixel intensities were equal to the bulk average pixel intensity for each element. For each element, 30 trials were run with random grid areas chosen. On average it takes 4 randomly selected Si areas, 5 randomly selected Mg areas, and 6 randomly selected Na areas to give an average within 2.5% of the bulk pixel intensity for each element, which gives an average pixel intensity within the 95% confidence interval of the bulk pixel intensity. When the pixel intensities are chosen from random grid areas from all three elements for 30 trials, it takes an average of 8 grid areas to reach a pixel intensity within a 95% confidence interval of the bulk pixel intensity.

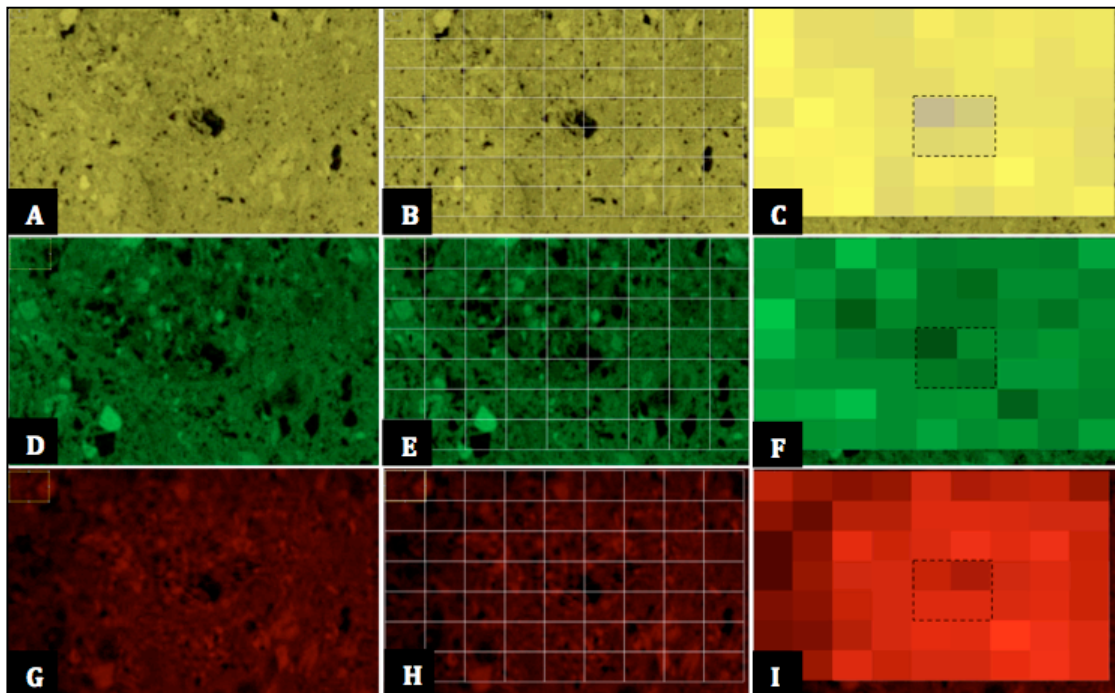


Figure 4.9 EDS element maps for Si (yellow), Mg (green), and Na (red) on LIBS Round 1, Location 2. (A), (D), and (g) show the full resolution area; (b), (e), and (h) show the 7x9 grid of LIBS spot size analysis areas; (c), (f), and (i) show a representative color scale of the changes in each element over the grid on the scale of the LIBS spot size. The black dashed line outlines the areas that covered the LIBS sampling location and thus are not included in the calculations of matrix intensities.

The results of the EDS sampling study can be supported with analysis of real LIBS data based on the sampling surface of the meteorite. Taking random groups of LIBS analyses from the 10 matrix sampling locations on the meteorite, it was found that an average of 4 Si locations, 4 Mg locations, and 3 Na locations are needed to calculate an emission peak area within 10% of the bulk matrix area for each element. Putting all three elements together, it would take an average of 4 LIBS analysis locations to get matrix emission peak areas that match the bulk peak area for Si, Mg, and Na. Because these calculations were completed on the matrix analysis locations, these results should only apply when the LIBS spot size is bigger than the grain size of the target being analyzed. Not enough clast analyses were observed to be able to perform a randomized

study, but the EDS study was further explored through calculation of matrix and clast average LIBS peak areas and their standard deviations. The results of this exercise show there are not enough points to distinguish the clasts from the matrix in LIBS data. This suggests more LIBS analysis locations than the four on this meteorite would be needed to determine a clast composition from a matrix composition. These data are not conclusive in deciding the number of points needed to give an accurate bulk composition because the PLS and/or univariate analysis techniques are not included. However, this is an important step toward helping the ChemCam team recognize which observed qualities in LIBS data may be genuine and which ones may be artifacts of the sampling of the instrument.

To examine the effect of LIBS spot size in clasts larger than the LIBS spot, the clast from LIBS Round 1, Location 10 was analyzed for pixel intensity in Si, Mg, and Na EDS images using the same methods as described above. The clast is made up of grains of a generally homogeneous, small size, with the exception of a large grain in the upper portion of the clast. To explore the elemental variation within a clast, LIBS spot size pixel intensity analyses were performed on the interior of the clast (Figures 4.10-4.11). On the large grain, Si measurements varied only 15% between the lowest and highest measured intensities. Because LIBS is a three-dimensional analytical technique where multiple laser pulses are taken in a single location, the large grain's difference in Si abundance may be limited to a few higher-Si shots as the laser ablates material at depth, possibly passing through the grain. Figure 4.11 shows that the large grain in the clast has slightly higher Si and much higher Na pixel intensities than the other areas of the clast, while the Mg pixel intensity is much lower in the grain. This contributes to the high percent difference seen in the Mg measurements of the clast. Because the large grain is

dark-toned in the EDS Mg map, it is expected to have much lower Mg than the rest of the clast. Using Mg as an indicator of composition change is most appropriate for clasts like the one studied here due to its large spread in pixel intensities depending on the location of the analysis area. As applied to ChemCam on Mars, tracking the change in any element that varies greatly across a sample as Mg compositions vary here may help indicate the presence of grains that may not be resolvable by the Remote Micro-Imager (RMI) images that accompany LIBS analyses. EPMA analysis was done using wavelength dispersive spectroscopy (WDS) to analyze six micron-scale locations within this clast, and the quantitative data for each element can be compared to this semi-quantitative study. From the six WDS analysis locations, Si is shown to vary by only 7% while Mg and Na vary by more than 100% throughout the clast. It is important to keep in mind the scale difference between EPMA (micron to nm spot size) and LIBS (350-500 micron spot size) suggesting that the variation in composition seen by LIBS would be much less than that seen by EPMA.

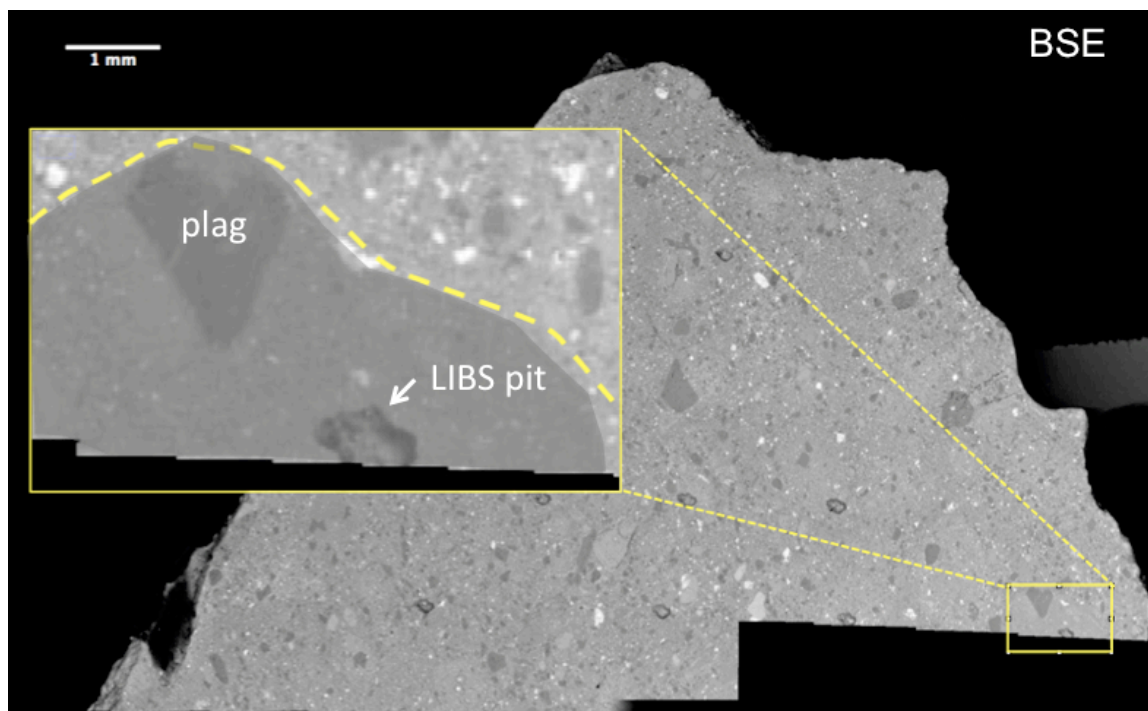


Figure 4.10 Backscattered Electron (BSE) image created after LIBS analysis on the NWA 7034 sample. The clast is outlined in a dashed yellow line and darkened in the inset (note that the entire clast is not shown). LIBS Round 1, Location 10 is visible in the lower center of the inset. EDS images for this region were used to calculate changes in pixel intensity for Si, Mg, Na, Al, and Ca on the LIBS spot size scale.

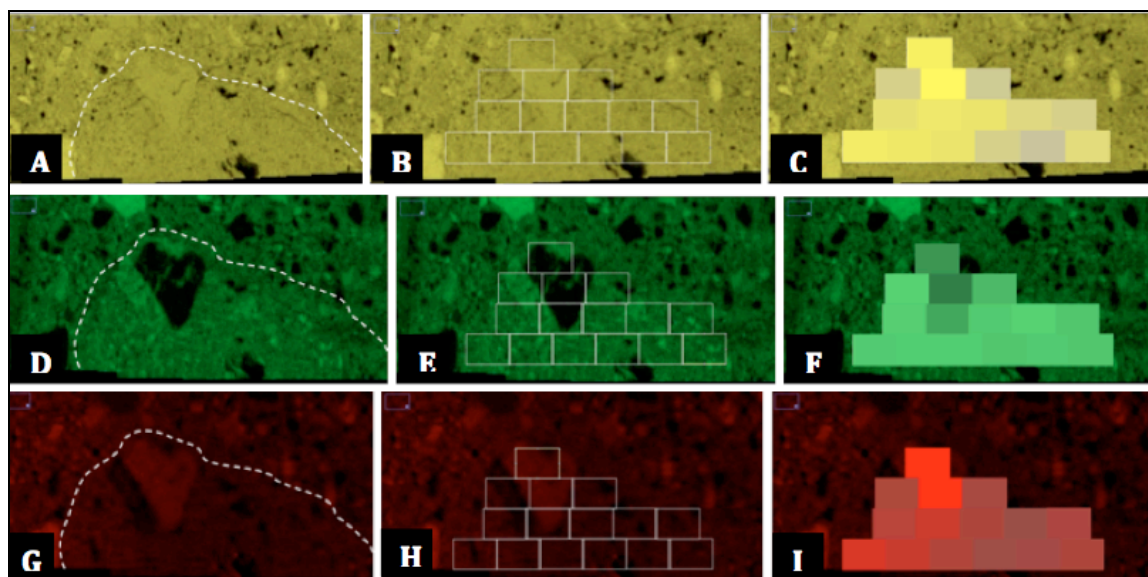


Figure 4.11 EDS maps of Si (yellow), Mg (green), and Na (red) images of LIBS Round 1, Location 10. (a), (d), and (g) show the original EDS element maps with the clast outlined in a white dashed curve; (b), (e), and (h) show the overlying grid of LIBS spot size analysis areas; (c), (f), and (i) show a representative color scale of the changes in each element over the grid on the scale of the LIBS spot size.

As a comparison between the pixel intensities measured for the matrix and an adjacent clast in this sample, a pixel intensity analysis of LIBS-sized areas in the matrix that cross into a clast can be performed with these same EDS images. The average pixel intensities and their standard deviations across the matrix and through a clast can show if a compositional difference can be detected between two adjacent materials on the LIBS spot size scale (Figures 4.12-4.13). The clast and matrix in this portion of the sample was not analyzed by LIBS. However, the EDS analysis shows similar pixel intensities in the clast as in the matrix (Table 4.1). This clast also contains a few large grains that appear darker than the rest of the clast in the BSE image in Figure 4.10, indicating a higher abundance of elements with low atomic numbers (such as Na). These large grains have slightly higher Si, much higher Na, and much lower Mg abundances than the rest of the clast (Fig. 4.13). It can also be seen that the Mg content of the clast varies more than the Si and Na content. Figure 4.13(C,F,I) show higher Mg and lower Na pixel intensities in the center of the clast and relatively uniform Si intensities throughout the clast and matrix. Given that this clast it is distinguished from the matrix despite being so similar in pixel intensity to the matrix, it is likely that any felsic or lighter toned clasts elsewhere in the sample would be similarly distinguishable from the matrix in LIBS data, as long as the grains are larger than the LIBS spot size. Table 4.1 shows that the clast and matrix average intensities are similar within one standard deviation; however, these measurements only reflect analysis of the surface of the sample. More observation points and depth profiles into the sample with LIBS would likely lower the standard deviation of the element abundance values enough to distinguish between matrix and clast compositions (e.g. McCanta et al., 2013).

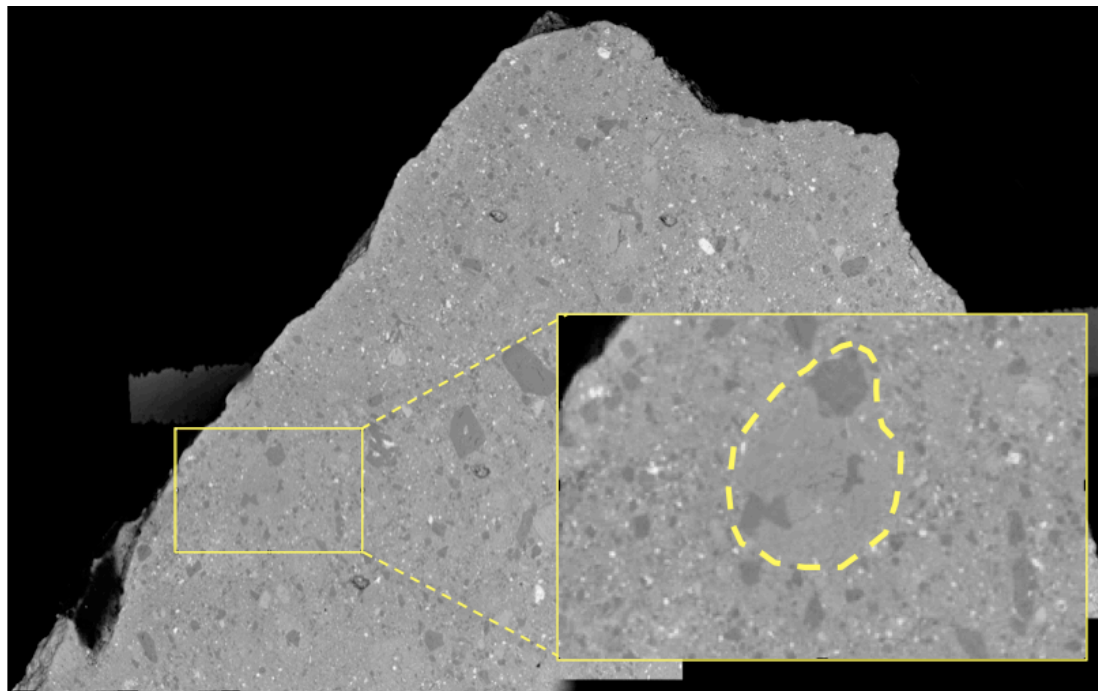


Figure 4.12 Backscattered Electron (BSE) image created after LIBS analysis on NWA 7034. The clast is outlined in a dashed yellow line in the inset. This area was used in the EDS element maps to calculate changes in pixel intensity for Si, Mg, Na, Al, and Ca on the scale of the LIBS spot.

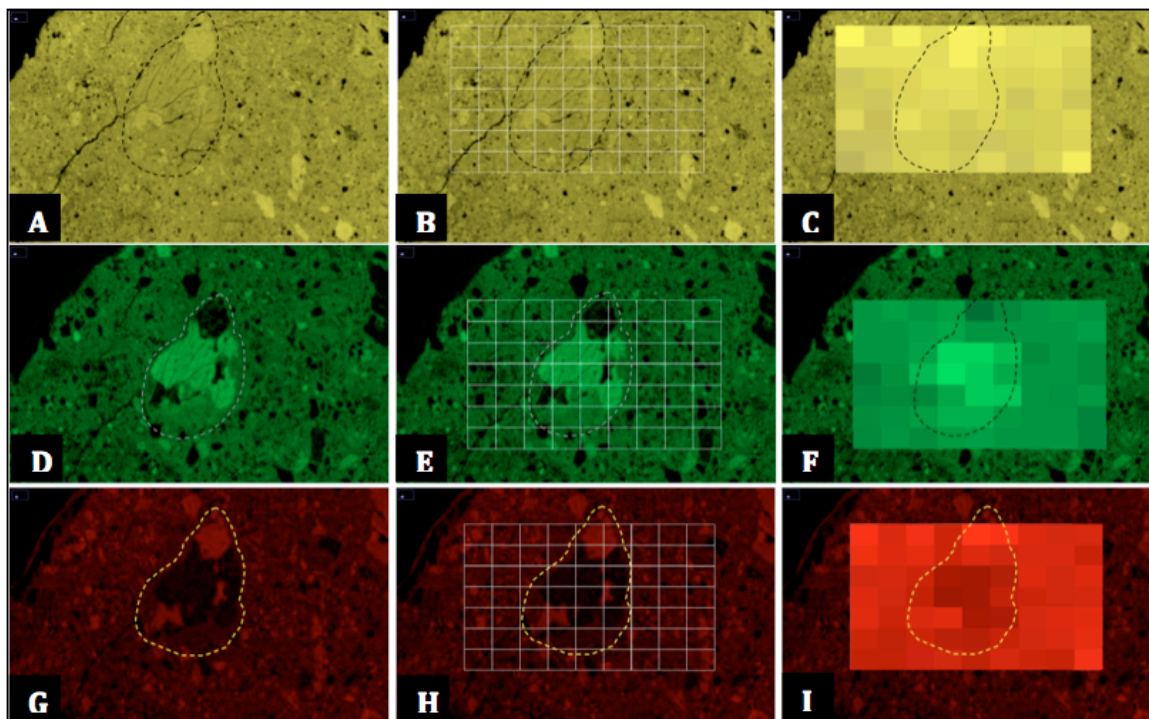


Figure 4.13 EDS element maps for Si (yellow), Mg (green), and Na (red) images of NWA 7034 matrix and clast as seen by EDS analysis. (A), (D), and (G) show the original EDS element maps with the clast outlined in a dashed curve; (B), (E), and (H) show the overlying grid of LIBS spot size analysis areas; (C), (F), and (I) show a representative color scale of the changes in each element over the grid on the scale of the LIBS spot size.

	<i>Matrix</i>					<i>Clast</i>				
	Avg.	Std. Dev.	Min.	Max.	% Diff.	Avg.	Std. Dev.	Min.	Max.	% Diff.
Si	76.9	5.55	65.3	93.8	35.9	79.1	4.66	71.4	89.5	22.5
Mg	20.9	1.81	15.9	23.7	39.2	27.2	7.40	13.4	42.7	105
Na	14.9	1.75	11.7	19.6	50.7	13.0	3.42	8.40	22.5	91.2
Al	14.9	3.37	9.71	22.0	77.6	12.5	5.54	4.05	29.7	152
Ca	19.7	3.39	11.7	30.1	88.4	20.2	4.50	13.0	28.7	75.4

Table 4.1 Si, Mg, Na, Al, and Ca pixel intensity measurements for the matrix and clast in Figure 4.12.

To test the discrepancy between data processing uncertainty and sampling uncertainty, the number of hypothetical LIBS spots needed to give a bulk matrix pixel intensity within 2.5% as calculated using the grids in Figure 4.9 was compared to the

number of actual LIBS matrix observations needed to give a bulk composition within 2.5% of the given LIBS composition for NWA 7034. Pixel intensities were measured from the EDS maps and averaged in random sets of two, three, four, and so on observations with 30 iterations of random sampling, as described above. The process was repeated using the average LIBS compositions at the matrix locations observed in this study. For the EDS data, an average of five data points were needed to give an average pixel intensity within a 95% confidence interval of the bulk pixel intensity, while for LIBS data, an average of four data points were needed to give a composition or pixel intensity within a 95% confidence interval of the bulk composition for Si, Mg, and Na. This supports the finding by McCanta et al. (2013) that LIBS observations where the laser spot size is larger than the grain size need a low number of observation locations to get an accurate bulk composition. A comparable study could not be completed using clast LIBS data because there were not enough LIBS observation points acquired on clasts. Instead, the LIBS spectral peaks were investigated to further understand how peak area, which is an indication of composition, changes between matrix and clast observation locations.

The results of the LIBS spectral peak area calculations are shown in Table 4.2. Si and Mg follow the same pattern of clast peak areas greater than matrix peak areas, which are both greater than the peak areas measured for observation locations that hit both matrix and clast. Fe and Ca show an opposite trend where clast peak areas are the smallest, followed by matrix peak areas and then areas that hit both clast and matrix. Na, Al, and K all show different patterns that do not correlate with any other elements. The contribution of matrix versus clast compositions to LIBS observations that hit both matrix

and clast is outside the scope of this project, so only the matrix and clast results will be discussed here. Al, Fe, Ca, and K all show lower clast peak areas than their respective matrix areas, while Si and Mg are opposite. Tracking these different trends may help distinguish the difference between matrix and clast locations in LIBS data for similar targets found on Mars. If clasts are visible in RMI images of future targets that may be similar to NWA 7034, these images can be used to ensure LIBS locations are properly labeled as clast, matrix, or both. If clast sizes are too small to be seen by RMI images, or their coloration does not have enough contrast to stand out in the images, it will be more difficult to distinguish between clast and matrix points. Further investigation of the NWA 7034 LIBS data set in comparison with Mars targets shows what can be expected if a sample as heterogeneous as the martian meteorite are observed by ChemCam.

	Matrix	Clast	Both
Si	3.98×10^{-3}	7.35×10^{-3}	3.63×10^{-3}
Mg	1.72×10^{-2}	2.16×10^{-2}	1.59×10^{-2}
Na	1.98×10^{-2}	1.98×10^{-2}	1.59×10^{-2}
Al	2.80×10^{-3}	2.60×10^{-3}	2.87×10^{-3}
Fe	1.56×10^{-2}	1.17×10^{-2}	2.11×10^{-2}
Ca	2.34×10^{-2}	2.08×10^{-2}	2.92×10^{-2}
K	5.27×10^{-3}	4.4×10^{-3}	3.40×10^{-3}

Table 4.2 LIBS spectral peak areas measured from the first round of LIBS observations. Peak areas are calculated using the peak areas for all major emission lines of each given element.

4.4 Comparison of NWA 7034 and ChemCam targets Martian meteorite NWA 7034 is chemically and texturally similar to many materials observed in the *Curiosity* Gale crater landing site. The bulk composition of the meteorite is alkali basaltic, suggesting the materials at the sedimentary landing site have an igneous formation history. Light-toned materials that appear to be a range of feldspar minerals have been observed in Gale (Grotzinger et al., 2014) and are found in NWA 7034 as well. Sautter et al. (2014) created three categories of light-toned materials observed in Gale; Class 3, described as porphyritic rocks with elongated leucocratic crystals embedded in a dark-colored matrix, is most similar to NWA 7034. The type target for this class is Harrison (sol 514) (Figure 2.9). Along with Harrison, the ChemCam targets Jake M (sols 45 and 48), Ashuanipi (sol 337), and La Reine (sol 346) were chosen to compare to NWA 7034 based on their spectral similarity as compared in a Sammon's map (Figure 4.14). The Sammon's map is a measure of spectral similarity that projects data along the axes of greatest variation, similar to principal components analysis (PCA) and independent component analysis (ICA). Sammon's maps are used as a tool to determine which types of rocks are similar as opposed to identifying specific rock types based on where the samples cluster (Lasue et al., 2011). In the Sammon's map used in this study, the spectra for the targets were compared and the targets were plotted according to the similarity of their SiO₂ (x-axis) and Na₂O (y-axis) peak intensities.

more ChemCam targets to compare with NWA 7034. To better understand how a target similar to NWA 7034 might appear to ChemCam, its composition and texture may be compared to other Gale rock targets. Thus far, no targets in Gale crater have been found that show a clearly brecciated texture, so the Jake M target will be used as a comparison to the heterogeneous textures of NWA 7034 in this study.

Data from a typical ChemCam analysis on a target includes an RMI mosaic, preliminary PLS results, an examination of trace elements present, and any trends observed in shot-to-shot spectra. PLS results for Jake are shown in Tables 3.3 and 3.4

	SiO ₂	TiO ₂	Al ₂ O ₃	FeOT	MgO	CaO	Na ₂ O	K ₂ O	Total
RMSEP	7.1	0.55	3.7	4	3	3.3	0.7	0.9	10.1
Jake 1	63.9	0.35	6.9	19.8	2.5	1.7	3.5	1.5	100.2
Jake 2	50.1	2.11	9.3	21.7	2.4	6.2	1.8	0.3	93.9
Jake 3	69	0.42	14.2	15.3	0.3	3.3	4.1	2	108.6
Jake 4	54.5	0.61	10.9	14.2	2.6	5	3	1.4	92.2
Jake 5	48.4	1.05	9	15	3.8	8.5	2.9	0.9	89.6

Table 4.3 Jake M PLS results color-coded to highlight differences between LIBS observation locations.

	SiO ₂	TiO ₂	Al ₂ O ₃	FeOT	MgO	CaO	Na ₂ O	K ₂ O	Total
RMSEP	7.1	0.55	3.7	4	3	3.3	0.7	0.9	10.1
Jake 11	63.6	0.62	11.7	13.6	1.5	6.5	4.4	1.9	103.8
Jake 12	55	1.59	10.1	19.6	1.3	6	2.6	1.1	97.3
Jake 13	60.2	0.86	11.4	15.4	0.4	5.5	3.2	1.8	98.8
Jake 14	46	0.83	8	14.9	3.1	9.2	2.8	0.8	85.6
Jake 15	67.6	0	12.8	9.8	0	3	5.6	3	101.8
Jake 16	58.1	1.35	9.8	19.4	1.6	7.4	2.9	0.9	101.5
Jake 17	59.2	0.95	10.5	18	0.7	6.4	3.5	1.7	101
Jake 18	53.1	1.18	9	16.2	2	8.1	3	0.8	93.4
Jake 19	49.9	0.98	6.9	15.7	5.9	14.6	2.6	0.7	97.3

Table 4.4 PLS results for the second LIBS observation of Jake M color-coded to highlight differences between LIBS observation locations.

Examination of the PLS results shows variation in abundance in every element above its RMSEP, suggesting that this rock is heterogeneous. However, it was only after further investigation of the target's RMI images that this heterogeneity was recognized as sampling differences rather than data processing uncertainties. Despite having a brecciated texture containing a variety of clasts and grain sizes, if NWA 7034 were a rock target observed by ChemCam on Mars, it would appear similarly heterogeneous. Its alkali basaltic bulk composition might have been seen as average in relation to the compositions seen on Mars. However, the heterogeneous texture of NWA 7034 might have been identified in RMI images, which shows the importance that geologic context images can have for interpreting measured chemistry.

5. CONCLUSION

Because of its similarity to Gale crater materials, the basaltic breccia meteorite NWA 7034 can help bridge the gap between *in situ* and meteoritical martian studies. By analyzing this meteorite with the ChemCam engineering model on Earth, it may be directly compared to similar data being obtained by ChemCam on Mars. The LIBS observations on NWA 7034 show that the two clasts examined in detail here have shot-to-shot compositions that cluster separately, with standard deviations that do not overlap. The relationship between grain size and laser spot size is shown to be important in determining chemical compositions; a bulk composition can be found with only five observation locations as long as the grain size is smaller than the spot size. While the accuracy of processed LIBS data is beyond the scope of this project, it was found that a combination of PLS and univariate analysis gave chemical compositions within error of the EPMA bulk data previously reported for the meteorite. If NWA 7034 had been a ChemCam target in Gale crater, both the PLS results and RMI images would have shown the larger clast variations in the sample, assuming the exposed surface studied here would be visible to the rover. Applying these results to previously studied ChemCam targets shows no exact matches for the meteorite, although three targets were found to be chemically similar and one target was found to be texturally similar. This study demonstrates viable methods for ascertaining textural and chemical heterogeneity in rock targets analyzed by ChemCam and may help to guide sampling strategies as the MSL mission continues to analyze rocks in Gale crater on Mars.

6. REFERENCES

- Agee, C. B. et al. (2013) Unique Meteorite from Early Amazonian Mars: Water-rich Basaltic Breccia Northwest Africa 7034. *Science* **339**, 780-785.
- Boynton, W. V. et al. (2007) Concentrations of H, Si, Cl, K, Fe, and Th in the low- and mid-latitude regions of Mars. *Journal of Geophysical Research* **112**, E12S99.
- Cartwright, J. A. et al. (2014) Modern atmospheric signatures in 4.4 Ga Martian meteorite NWA 7034. *Earth and Planetary Science Letters* **400**, 77-87.
- Clegg, S. M. et al. (2009) Multivariate analysis of remote laser-induced breakdown spectroscopy spectra using partial least squares, principal component analysis, and related techniques. *Spectrochimica Acta* **64**, 79-88.
- Clegg, S. M. et al. (2014) Expansion of the ChemCam Calibration Database. *45th Lunar and Planetary Science Conference*, #2378.
- Dell'Aglio, M. et al. (2014) Laser Induced Breakdown Spectroscopy of meteorites as a probe of the early solar system. *Spectrochimica Acta Part B* **101**, 68-75.
- Fabre, C. et al. (2011) Onboard calibration igneous targets for the Mars Science Laboratory Curiosity rover and the Chemistry Camera laser induced breakdown spectroscopy instrument. *Spectrochimica Acta Part B* **66**, 280-289.
- Fabre, C. et al. (2014) In situ calibration using univariate analyses based on the onboard ChemCam targets: first prediction of Martian rock and soil compositions. *Spectrochimica Acta Part B* **99**, 34-51.
- Gellert, R. et al. (2006) Alpha Particle X-Ray Spectrometer (APXS): Results from Gusev crater and calibration report. *Journal of Geophysical Research* **111**, E02S05.

- Grotzinger, J. P. et al. (2014) A Habitable Fluvio-Lacustrine Environment at Yellowknife Bay, Gale Crater, Mars. *Science* **343** DOI: 10.1126/science.1242777.
- Humayun, M. et al. (2013) Origin and age of the earliest Martian crust from meteorite NWA7533. *Nature* **503**, 513-516.
- Korotev, R. L. et al. (2013) Elemental and oxygen isotopic composition of martian mafic regolith breccia NWA 7475. *76th Annual Meteoritical Society Meeting*, #5046.
- Lanza, N. L. et al. (2012) Examining natural rock varnish and weathering rinds with laser-induced breakdown spectroscopy for application to ChemCam on Mars. *Applied Optics* **51**, B74-B82.
- Lasue, J. et al. (2011) Nonlinear mapping technique for data visualization and clustering assessment of LIBS data: application to ChemCam data. *Analytical and Bioanalytical Chemistry* **400**, 3247-3260.
- Maurice, S. et al. (2012) The ChemCam Instrument Suite on the Mars Science Laboratory (MSL) Rover: Science Objectives and Mast Unit Description. *Space Science Reviews* **170**, 95-166.
- McCanta, M. C. et al. (2013) Testing the veracity of LIBS analyses on Mars using the LIBSSIM program. *Planetary and Space Science* **81**, 48-54.
- McCubbin, F. M. et al. (2014) Alteration of sedimentary clasts in martian meteorite Northwest Africa 7034. *77th Annual Meteoritical Society Meeting*, #5099.
- McSween Jr., H.Y. (1985) SNC meteorites: Clues to Martian petrologic evolution? *Reviews of Geophysics*. **23**, 391-416.
- Papike, J.J. et al. (2009) Silicate mineralogy of martian meteorites. *Geochimica et Cosmochimica Acta* **73**, 7443-7485.

- Santos, A. R. et al. (2015) Petrology of igneous clasts in Northwest Africa 7034: Implications for the petrologic diversity of the martian crust. *Geochimica et Cosmochimica Acta* **157**, 56-85.
- Sautter, V. et al. (2014) Direct evidence for Si-rich crust in the southern hemisphere of Mars: Implications for Noachian magmatism. Submitted.
- Schröder, S. et al. (2012) LIBS studies of ferric salts in frozen solutions under Martian conditions. *43rd Lunar and Planetary Science Conference*, #1980.
- Sobron, P. et al. (2012) Extraction of compositional and hydration information of sulfates from laser-induced plasma spectra recorded under Mars atmospheric conditions – Implications for ChemCam investigations on Curiosity rover. *Spectrochimica Acta Part B* **68**, 1-16.
- Stolper, E. M. et al. (2013) The Petrochemistry of Jake_M: A Martian Mugearite. *Science* **341**, DOI: 10.1126/science.1239463.
- Thompson, J. R. et al. (2006) Remote laser-induced breakdown spectroscopy analyses of Dar al Gani 476 and Zagami Martian meteorites. *Journal of Geophysical Research* **111**, DOI: 10.1029/2005JE002578.
- Tucker, J. M. et al. (2010) Optimization of laser-induced breakdown spectroscopy for rapid geochemical analysis. *Chemical Geology* **277**, 137-148.
- Wiens, R. C. et al. (2002) Combined remote mineralogical and elemental identification from rovers: Field and laboratory tests using reflectance and laser-induced breakdown spectroscopy. *Journal of Geophysical Research* **107**, DOI: 10.1029/2000JE001439.

Wiens, R. C. et al. (2012) The ChemCam Instrument Suite on the Mars Science Laboratory (MSL) Rover: Body Unit and Combined System Tests. *Space Science Reviews* **170**: 167-227.

Wiens, R. C. et al. (2013) Pre-flight calibration and initial data processing for the ChemCam laser-induced breakdown spectroscopy instrument on the Mars Science Laboratory rover. *Spectrochimica Acta Part B* **82**, 1-27.

Wiens, R. C. and Maurice, S. (2015) ChemCam: Chemostratigraphy by the First Mars Microprobe. *Elements* **11**, 33-38.